

Response to reviewer's comments

Anonymous Referee #1:

Major comments:

The manuscript entitled "Assessing contributions of natural surface and anthropogenic emissions to atmospheric mercury in a fast developing region of Eastern China from 2015 to 2018", investigated the temporal variations of GEM, and developed a receptor model based method to quantify the contribution of natural surface mercury emission. The quantification of emission sources are significant to understand global mercury cycle. The development of the receptor model is one significant output of this study. However, the approach and the results is doubtful.

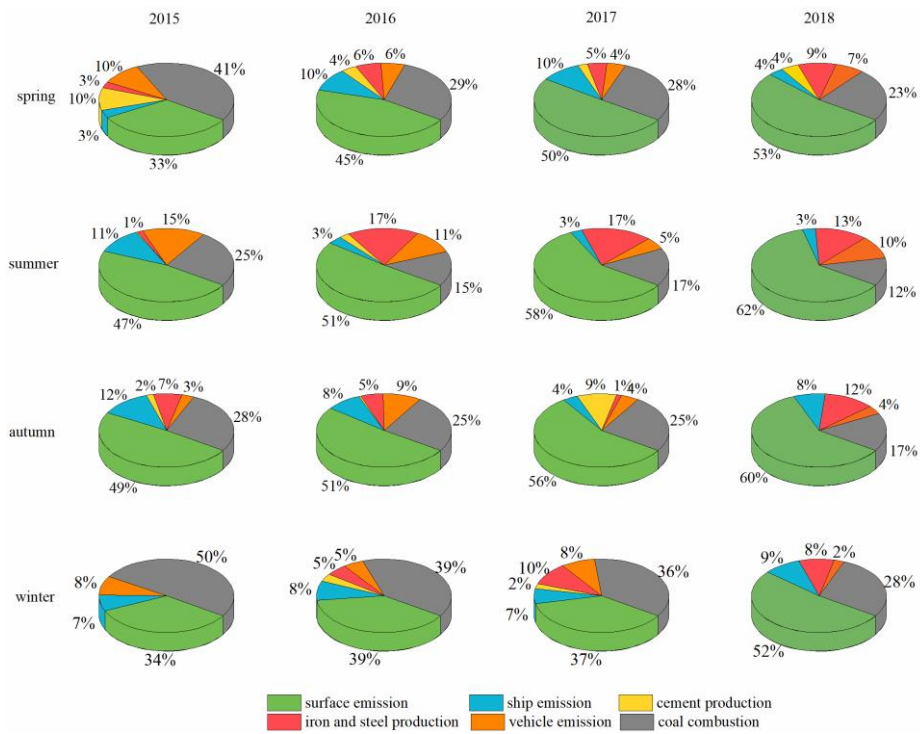
We sincerely thank for the reviewer's in-depth comments and helpful suggestions on this manuscript. Based on the specific comments, we have responded to all the comments point-by-point and made corresponding changes in the manuscript as highlighted in red color. The reviewer has raised a number of issues and we quite agree. We feel the substantial revisions based on the reviewer's comments have greatly improved the quality of this manuscript. Please check the detailed responses to all the comments as below.

Specific comments:

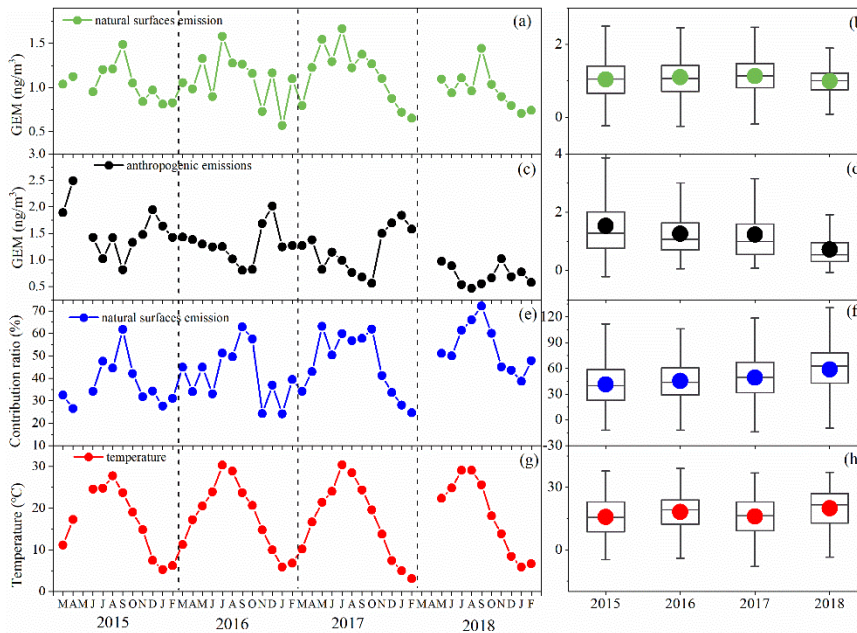
1. It is true that when temperature increase, we can observe high GEM and NH₃ emissions from natural sources. O₃ is a typical secondary pollutant formed from VOCs and NO_x, which mainly originates from photochemical reactions of anthropogenic pollutants and is impacted by temperature. The increase of temperature can also promote the generation of O₃ as well. But the simultaneous changes of these three are not entirely the contribution of natural source emissions. Take a simple example. Both NH₃ and mercury can participate between gas and particle. The increase of temperature will promote the generation of both NH₃ and GEM. In addition, high temperature in summer generally promote the generation of O₃. Thus, the simultaneous increase of NH₃, O₃, and GEM may occur due to atmospheric reaction process. Therefore, using O₃ and NH₃ as tracers of the natural emission of GEM will introduce a relative large uncertainty. The problem is that we do not know how large the uncertainty will be, because we cannot exhaust this kind of examples considering the variable sources and generation pathways of these three air pollutants and the complicated impact from temperature

Response: Thanks a lot for the reviewer's insightful suggestion. We agree that O₃ is not suitable as the tracer of natural emission as it is a typical secondary pollutant and shouldn't be used as a tracer for PMF modeling. Hence, we have removed O₃ and re-run the PMF model for the whole multi-year dataset. The new modeling results are shown in the following figures. We found that after the removal of O₃, the contributions of natural and anthropogenic sources to GEM from 2015 to 2018 didn't change much, hence the major conclusion hasn't been affected. In general, the contributions of natural sources to GEM increased slightly. For example, before removing O₃, the relative contribution of natural surface emissions to GEM increase from 36%

in 2015 to 53% in 2018. After removing O₃, its contribution increases from 41% in 2015 to 57% in 2018. In the revision, we replace Figure 5 and Figure 6 with the following two figures, and modified the corresponding specific contribution values.



Contributions of natural surface emissions and anthropogenic sources to atmospheric GEM in the four seasons during 2015 – 2018.



The monthly and annual GEM concentrations contributed by natural surface emissions (a-b) and anthropogenic emissions (c-d) from 2015 to 2018. (e-f) The monthly and annual

contribution of natural surface emissions to GEM concentrations from 2015 to 2018. (g-h)
The corresponding ambient temperature from 2015 to 2018.

2. The results are also confusing. The author stated that “As for the other resolved factors, . . . of Pb and SO₄²⁻” (Line 255-261). The explanation of the factors is too arbitrary and lacks enough support.

Response: We agree with the reviewer that the explanation of the factors is not sufficient. In the revision, we revised the sentences as “ As for the other resolved factors, the factor with high loadings of V and Ni evidently represented shipping emissions, because Ni and V have been considered as typical tracers of heavy oil combustion which has been commonly used in marine vessels (Viana et al., 2009). The factor with high loading of Ca was assigned to cement production as the raw materials used in cement production contain a large amount of calcium compounds. Moderate loadings of multiple species including Cr, Mn, and Fe were found in one factor which was identified as iron and steel production. The factor with high loading of NO was identified as vehicle emissions, as the major source of NO_x in the YRD region is mobile oil combustion (Tang et al., 2018). And the last factor was identified as coal combustion due to the high loadings of As and Se, and moderate contributions from Pb and SO₄²⁻. As, Se, and Pb were all typical tracers of coal combustion and the precursor of SO₄²⁻ (i.e. SO₂) also mainly derived from coal combustion.”

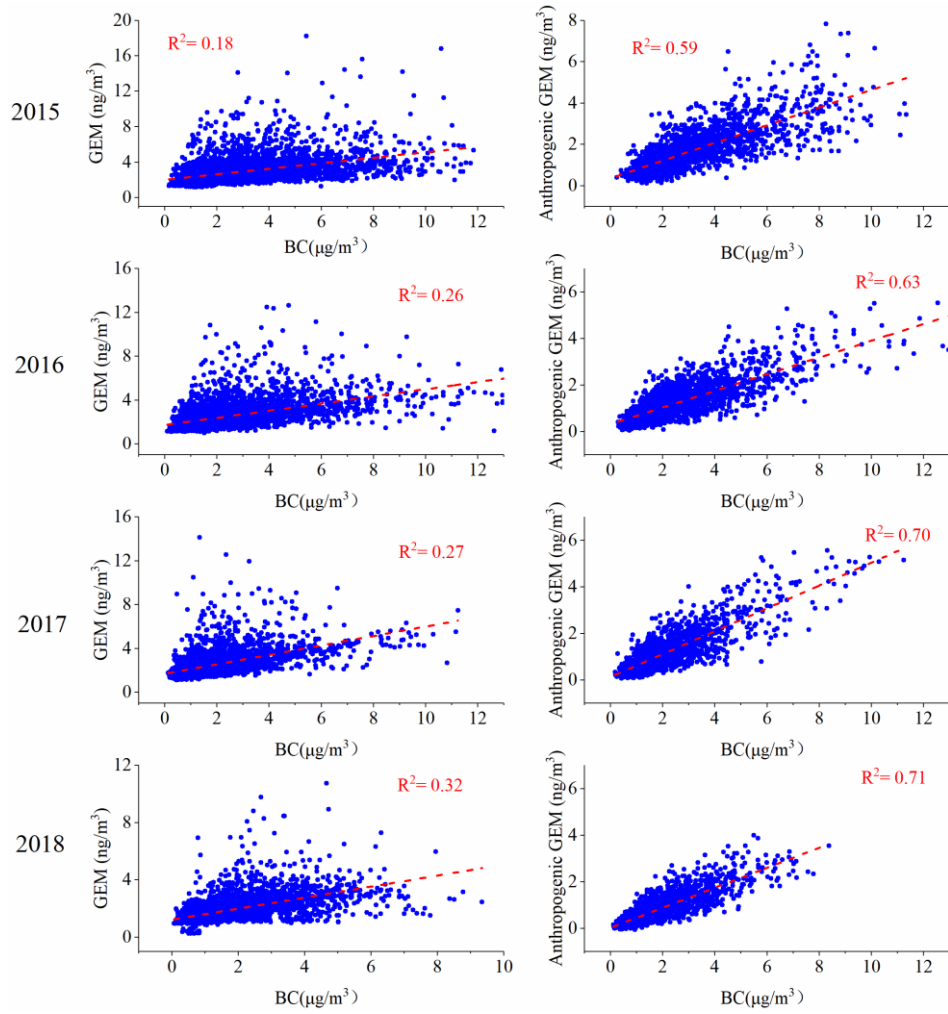
3. For example, the authors pointed out that the factor with high loadings of Ca was assigned to cement production. However, there are several anthropogenic Ca emission sources if the authors investigated the heavy metal emission inventory, such as the ferrous metal smelting. Ferrous metal smelting is also one significant emission sources around Shanghai. From this aspect, the anthropogenic sources resolved by using the developed model cannot be supported by the emission inventory.

Response: Thanks for the comment. According to the emissions inventories of China, non-ferrous metals smelting plants are mainly concentrated in Hunan, Yunnan, and Henan provinces (Liu et al., 2019). Hg emissions from non-ferrous metals smelting gradually decreased since 2004 in China, benefitting from the elimination of small-scale smelters and stringent SO₂ emission control measures (Wu et al., 2016). As for the YRD region, the recent emissions inventories show that the main emission sectors of GEM include coal-fired power plants, coal-fired industrial boilers, residential coal combustion, cement clinker production, iron and steel production, and mobile oil combustion, but very little from non-ferrous metal smelting (Tang et al., 2018). According to the emission inventories, the annual GEM emission from cement production in the YRD region is around 2.3 tons/year, accounting for about 13% of its total anthropogenic emissions (Tang et al., 2018). By considering the natural sources of GEM (Zhu et al., 2016) , the contribution of cement production to total GEM emissions should be lower than 13%. In this study, the seasonal contribution of cement production to the ambient GEM was estimated to be in the range of 2% - 10% at the study site. Hence, the PMF modeling results were generally consistent with the emission inventories.

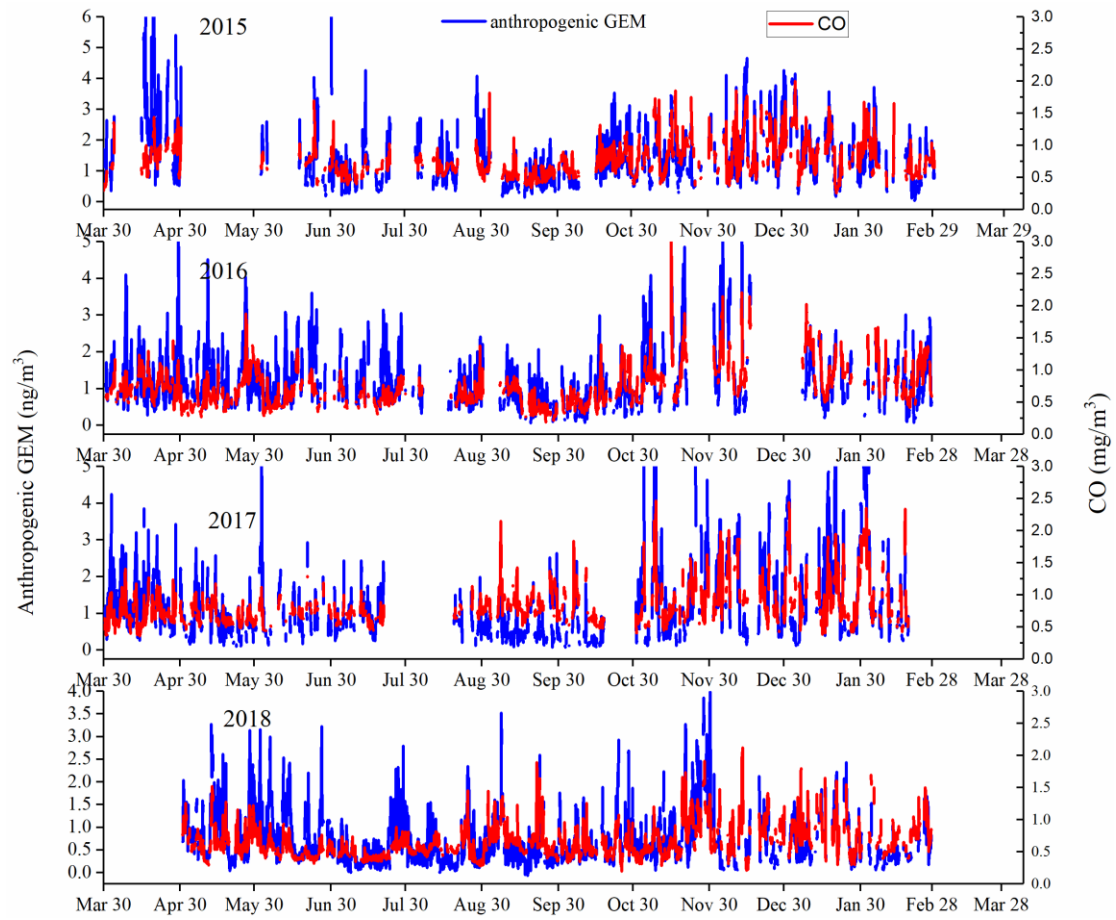
4. Due to the question of current receptor model and their definition of different factors, I think the authors need to carefully verify their results or use other source resolution methods to determine the sources.

Response: Thanks for the comments and we do agree with the reviewer that the results should be carefully verified. In this regard, we have conducted more analysis to verify the results of PMF model from several aspects.

First, we verified whether the separation of natural and anthropogenic GEM was credible or not, which was also the main focus of this study. To achieve this, the relationship between particulate black carbon (BC) and GEM concentrations was investigated. On the one hand, BC mainly derived from various combustion processes, which were also the main anthropogenic sources of atmospheric mercury. On the other hand, BC was never introduced into the PMF modeling. As shown in the figure below, the observed total GEM concentrations and BC concentrations only showed weak correlations. This was mainly due to the fact that besides anthropogenic sources, natural sources also contributed significantly to GEM. As a comparison, anthropogenic GEM concentrations (extracted from PMF results) showed much stronger correlations with BC from 2015 to 2018. In addition, the time series of anthropogenic GEM concentrations generally varied consistently with CO (shown in the figure below), which is also a tracer of fuel combustion. This suggests that the PMF results are credible and the separation of anthropogenic and natural GEM has been successfully achieved.

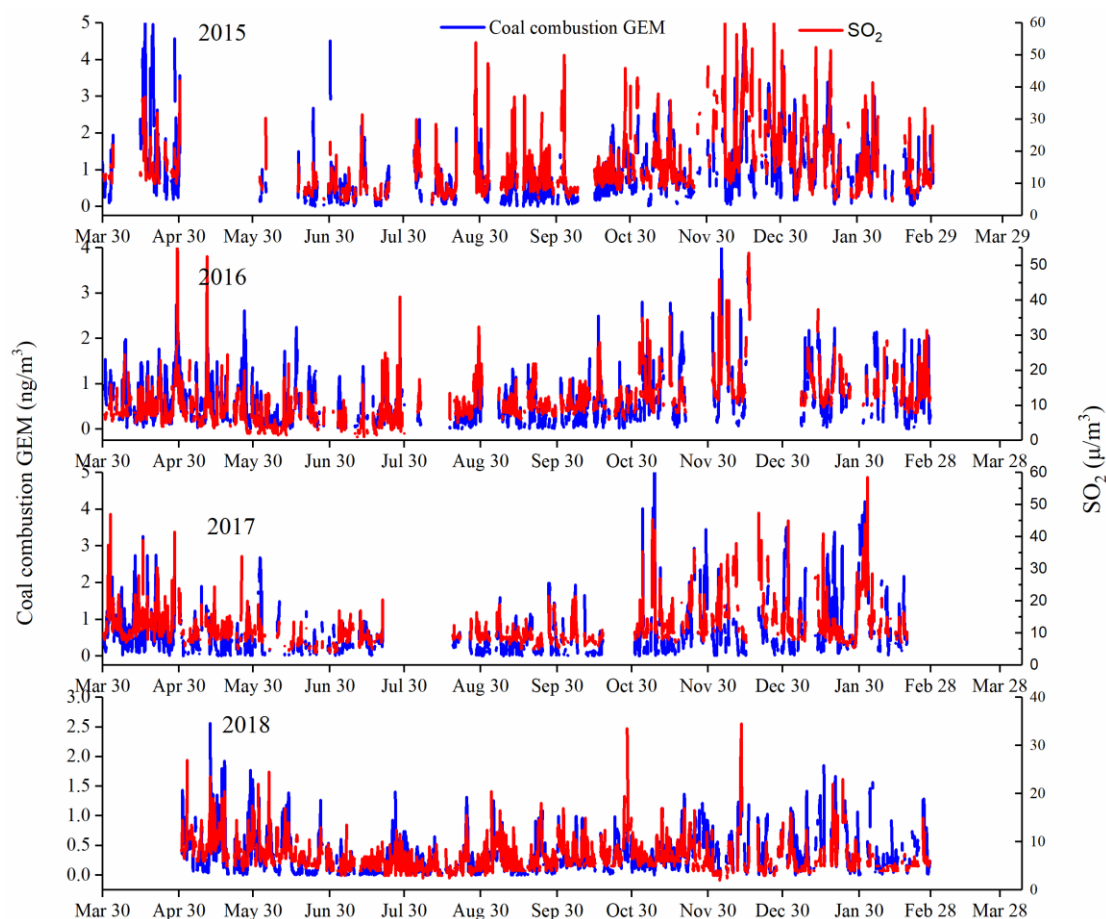


The relationship between observed GEM and BC, anthropogenic GEM (extracted from PMF results) and BC during 2015 – 2018



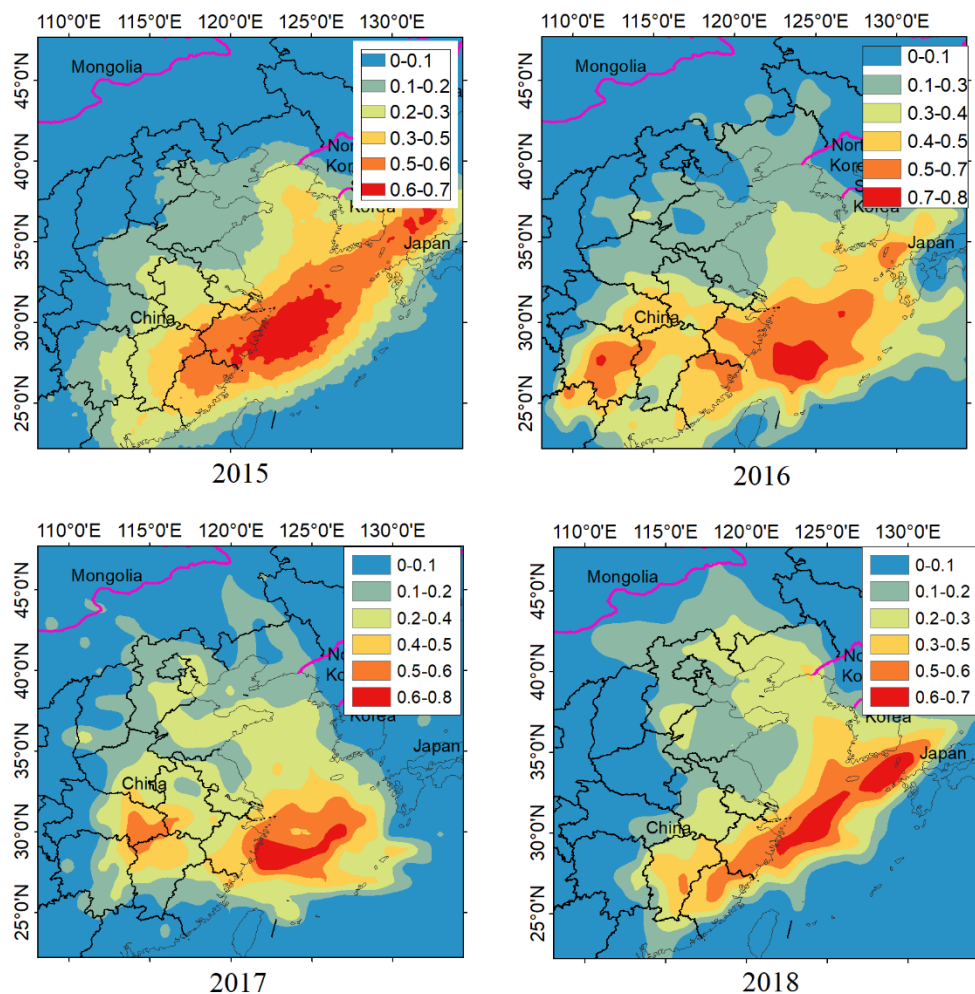
Time series of anthropogenic GEM and CO concentrations

Furthermore, as shown in the figure below, we examine the time series of coal combustion GEM (extracted from PMF results) and observed SO₂ from 2015 to 2018. It is found that the trend of coal combustion GEM is basically consistent with that of SO₂, which indicates that the coal combustion factor resolved by PMF is credible.



Time series of coal combustion GEM and SO₂ concentrations

To verify the resolved shipping emission factor from PMF modeling, we use the PSCF model to identify the potential source regions of the shipping GEM (extracted from PMF results) from 2015 to 2018. As shown in the figures below, the potential source regions are mainly located over coastal and oceanic areas, which suggests that the shipping factor resolved by PMF is credible.



Potential source regions of shipping GEM from 2015 to 2018

In the revised manuscript, we have added a paragraph about the verification of PMF results as below.

“In addition, the relationship between particulate black carbon (BC) and GEM concentration was investigated. On the one hand, BC mainly derived from various combustion processes, which were also the main anthropogenic sources of atmospheric mercury. On the other hand, BC was never introduced into the PMF modeling. As shown in Figure 5, the observed total GEM and BC concentrations only showed weak correlations. This was mainly due to the fact that besides anthropogenic sources, natural sources also contributed significantly to GEM. As a comparison, anthropogenic GEM concentrations (extracted from PMF results) showed much better correlations with BC from 2015 to 2018. In addition, the time-series of anthropogenic GEM concentrations generally varied consistently with CO, which was also a tracer of fuel combustion (Figure S28). All the evidences above corroborated that by using temperature and NH₃ as tracers for PMF modeling, the separation of anthropogenic and natural GEM can be successfully achieved.

As for the specific anthropogenic mercury sources extracted from PMF results, Figure S29 shows that the time-series of coal combustion GEM also varied consistently with SO₂, indicating that the coal combustion factor resolved by PMF was credible. As shown in Figure S30, the potential source regions of shipping GEM were found mainly over coastal and oceanic areas, indicating the shipping factor resolved in this study was also valid. Figure S31 and Figure S32 show that the PSCF signals of cement production GEM were relatively weak in the YRD region, while there were substantial high PSCF signals for iron and steel production GEM in Eastern China. All the results above collectively confirmed that the PMF results were robust."

References:

- Liu, K., Wu, Q., Wang, L., Wang, S., Liu, T., Ding, D., Tang, Y., Li, G., Tian, H., Duan, L., Wang, X., Fu, X., Feng, X., and Hao, J.: Measure-Specific Effectiveness of Air Pollution Control on China's Atmospheric Mercury Concentration and Deposition during 2013-2017, *Environmental science & technology*, 10.1021/acs.est.9b02428, 2019.
- Tang, Y., Wang, S. X., Wu, Q. R., Liu, K. Y., Wang, L., Li, S., Gao, W., Zhang, L., Zheng, H. T., Li, Z. J., and Hao, J. M.: Recent decrease trend of atmospheric mercury concentrations in East China: the influence of anthropogenic emissions, *Atmospheric Chemistry and Physics*, 18, 8279-8291, 10.5194/acp-18-8279-2018, 2018.
- Viana, M., Amato, F., Alastuey, A., Querol, X., Moreno, T., García Dos Santos, S., Herce, M. D., and Fernández-Patier, R.: Chemical Tracers of Particulate Emissions from Commercial Shipping, *Environmental science & technology*, 43, 7472-7477, 10.1021/es901558t, 2009.
- Wu, Q. R., Wang, S. X., Li, G. L., Liang, S., Lin, C. J., Wang, Y. F., Cai, S. Y., Liu, K. Y., and Hao, J. M.: Temporal Trend and Spatial Distribution of Speciated Atmospheric Mercury Emissions in China During 1978-2014, *Environmental science & technology*, 50, 13428-13435, 10.1021/acs.est.6b04308, 2016.
- Zhu, W., Lin, C.-J., Wang, X., Sommar, J., Fu, X., and Feng, X.: Global observations and modeling of atmosphere–surface exchange of elemental mercury: a critical review, *Atmospheric Chemistry and Physics*, 16, 4451-4480, 10.5194/acp-16-4451-2016, 2016.

Response to reviewer's comments

Anonymous Referee #2:

Major comments:

This study has analyzed data from multiyear measurements of the gaseous elemental mercury (GEM) concentration at a regional background site in eastern China and quantified the contribution of natural surface emission to GEM using the positive matrix factorization (PMF) model. The long-term observation data are valuable and the topic is of broad interests.

My major concern is the robustness of the PMF results. To what extent should we believe these results? The results need further verification. Figure 5 is one of the most important yields from this study. Suppose Figure 5 is basically correct, we can draw some important conclusions from this figure:

(1) Although cement production is believed to be one of the most important emission sources in China, it seems to contribute very little to GEM at this site. Could this be true?

(2) The current Hg emission inventories haven't considered ship emissions, but this emission source should be considered in the Hg emission inventory development, especially for coastal areas. This could be a very important finding if it is true.

(3) Iron and steel production has a large contribution to GEM concentration as well. Is this site under the influence of many large iron and steel plants (e.g., Baogang)?

If the contributions from different anthropogenic sources could be verified to some extent, it would be much easier for the readers to believe the contribution from natural sources. One possible approach for the verification that I can think of is to use the PSCF model to identify the potential GEM source regions from 2015 to 2018. If the key source regions for the monitoring site are consistent with the above conclusions (e.g., do not have many cement plants; have potential ship emissions from the seas or the rivers; have many iron and steel production activities; etc.), the robustness of the PMF model could be verified.

Overall, I think this manuscript is worth publishing on Atmospheric Chemistry and Physics after major revision.

We sincerely thank for the reviewer's in-depth comments and helpful suggestions on this manuscript. Based on the specific comments, we have responded to all the comments point-by-point and made corresponding changes in the manuscript as highlighted in red color. The reviewer has raised a number of issues and we quite agree. We feel the substantial revisions based on the reviewer's comments have greatly improved the quality of this manuscript. Please check the detailed responses to all the comments as below.

Specific comments:

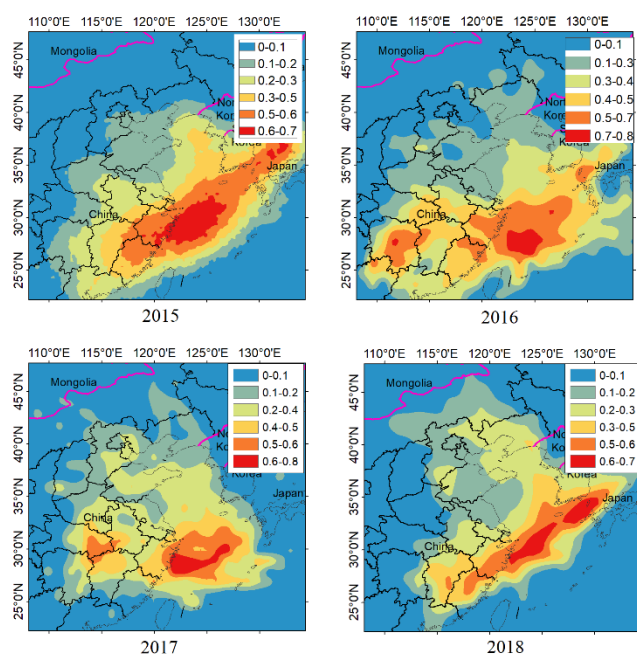
1. Although cement production is believed to be one of the most important emission sources in China, it seems to contribute very little to GEM at this site. Could this be true?

Response: We agree with the reviewer that cement production is one of the most important mercury sources in China. According to the emission inventories, the annual GEM emission from cement production in the YRD region is around 2.3 tons/year, accounting for about 13% of its total anthropogenic emissions (Tang et al., 2018). By considering the natural sources of GEM (Zhu et al., 2016), the contribution of cement production to total GEM emissions should be lower than 13%. In this study, the seasonal contribution of cement production to the ambient GEM was estimated to be in the range of 2% - 10% at the study site. Hence, the PMF modeling results were generally consistent with the emission inventories.

2. The current Hg emission inventories haven't considered ship emissions, but this emission source should be considered in the Hg emission inventory development, especially for coastal areas. This could be a very important finding if it is true.

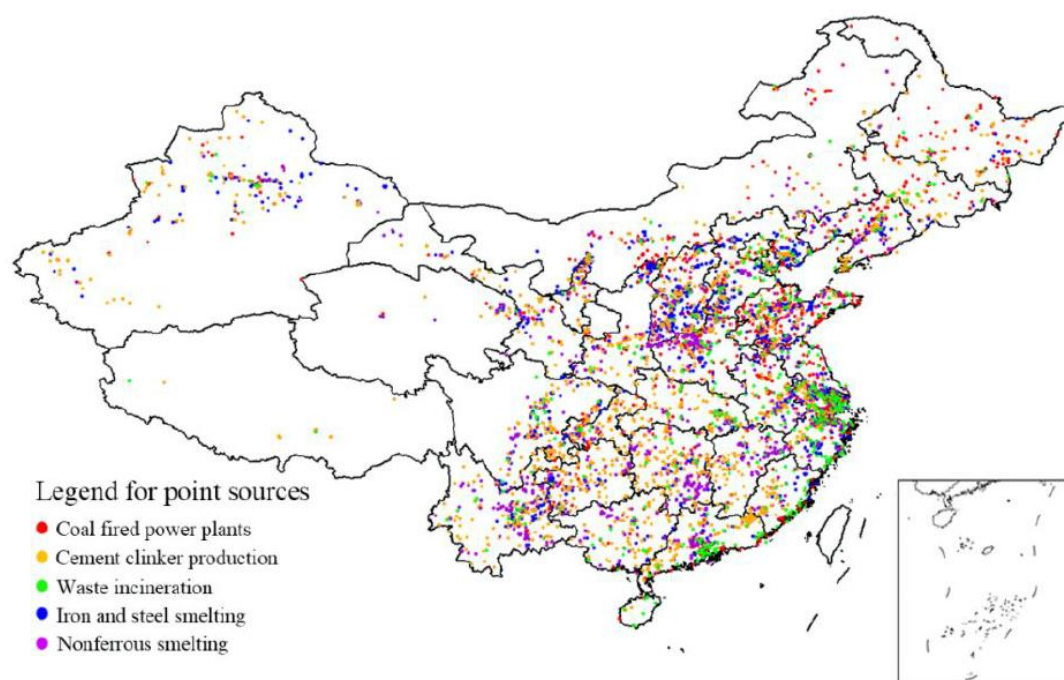
Response: Thanks for the comment. Shipping emissions are indeed important sources of air pollutants for the coastal areas, especially the East China Sea (Liu et al., 2017; Fan et al., 2016). However, as current Hg emission inventories haven't considered ship emissions as the reviewer mentioned, it is hard to verify the results of this study against the emission source data.

Instead, we plotted the PSCF maps of GEM contributed from shipping emissions extracted from the PMF modeling results as shown in the figure below. The results showed strong PSCF signals from the coastal and oceanic areas, indicating the shipping factor resolved in this study is valid. Again, this should be verified when shipping mercury emission inventory is available in the future.



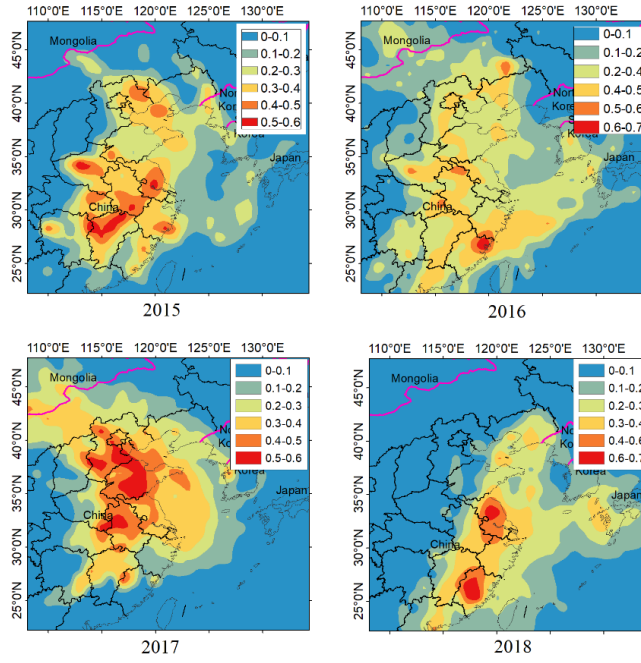
3. Iron and steel production has a large contribution to GEM concentration as well. Is this site under the influence of many large iron and steel plants (e.g., Baogang)?

Response: The figure below exhibit the geographical distribution of point sources in 2017 in China (Liu et al., 2019), which show that there are indeed many large iron and steel sites around our site (e.g., Baogang, Nangang, and Hanguang). According to the recent emission inventories, the contribution of iron and steel production accounts for about 7% of total anthropogenic GEM emissions (Tang et al., 2018). The seasonal contribution of iron and steel production to GEM ranged from 1% to 17% from 2015 to 2018 according to the PMF results. We believe that this site is under the influence of many large iron and steel plants.

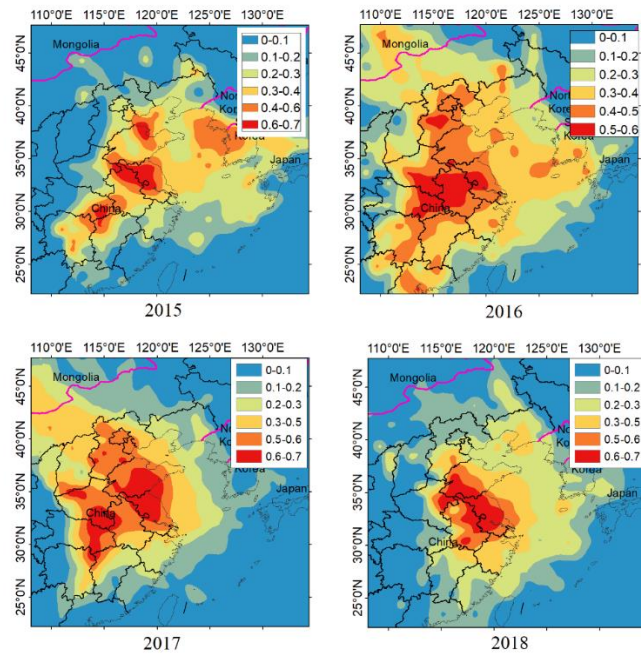


4. One possible approach for the verification that I can think of is to use the PSCF model to identify the potential GEM source regions from 2015 to 2018. If the key source regions for the monitoring site are consistent with the above conclusions (e.g., do not have many cement plants; have potential ship emissions from the seas or the rivers; have many iron and steel production activities; etc.), the robustness of the PMF model could be verified.

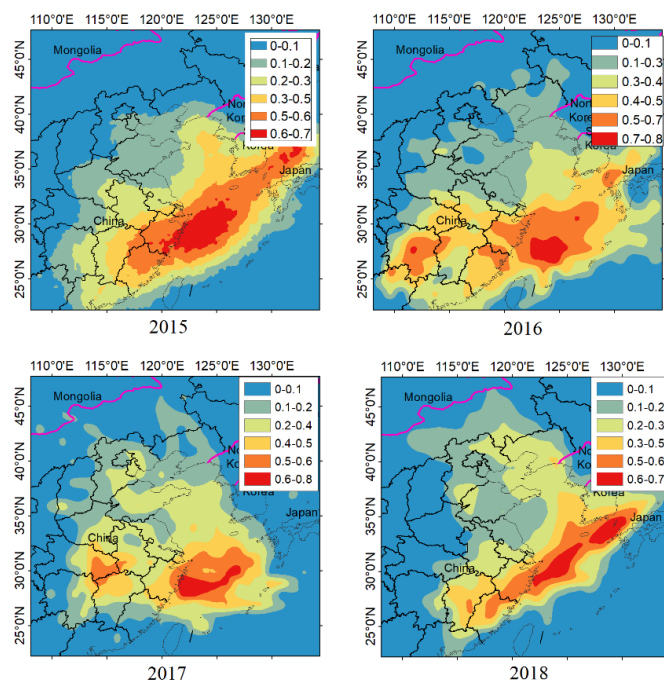
Response: According to the reviewer's suggestion, we have identified the potential source regions of the PMF modeled GEM from cement production, iron and steel production, and shipping activities during 2015 - 2018, respectively. As shown in the figures below, the PSCF signals of GEM from cement production in the YRD region are relatively weak, while there are substantial high PSCF signals for iron and steel production GEM in Eastern China. As for GEM from the shipping sector, most high PSCF signals are from the coastal and oceanic areas. These results suggest that the PMF results in this study are credible.



Potential source regions of GEM from cement production during 2015 - 2018



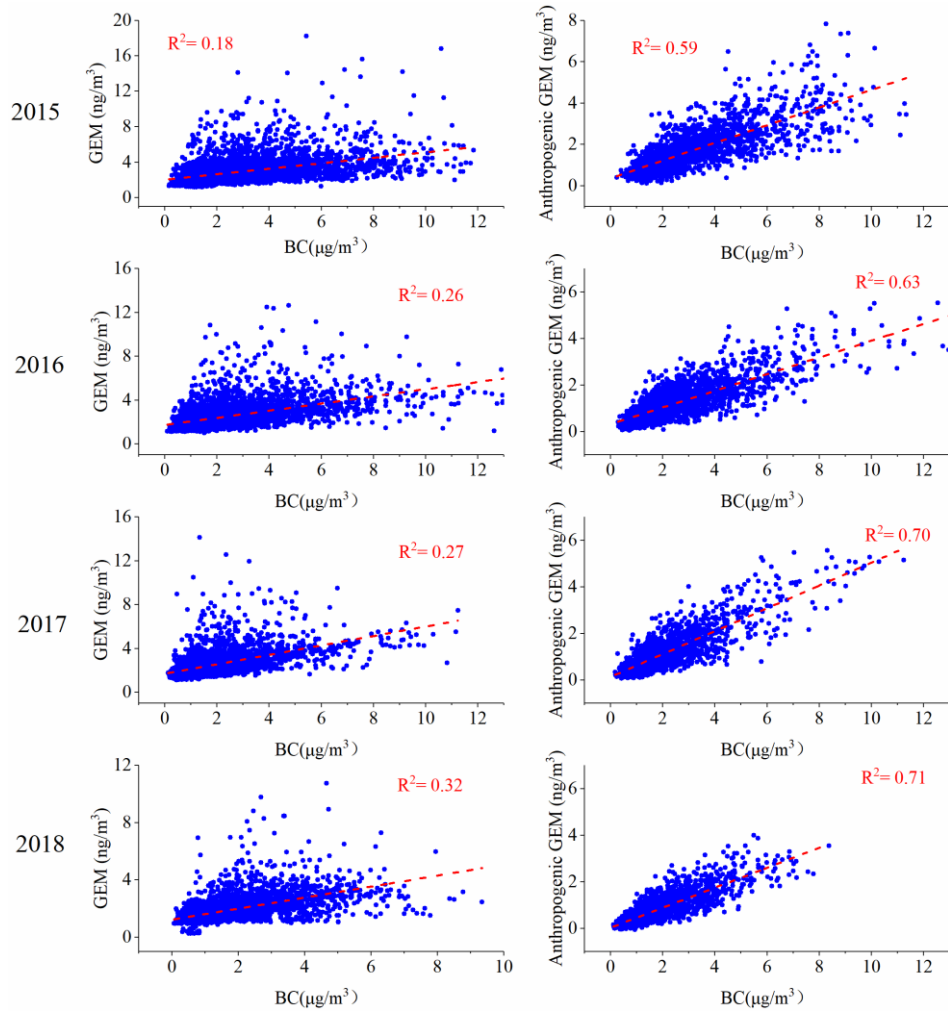
Potential source regions of GEM from iron and steel production during 2015 - 2018



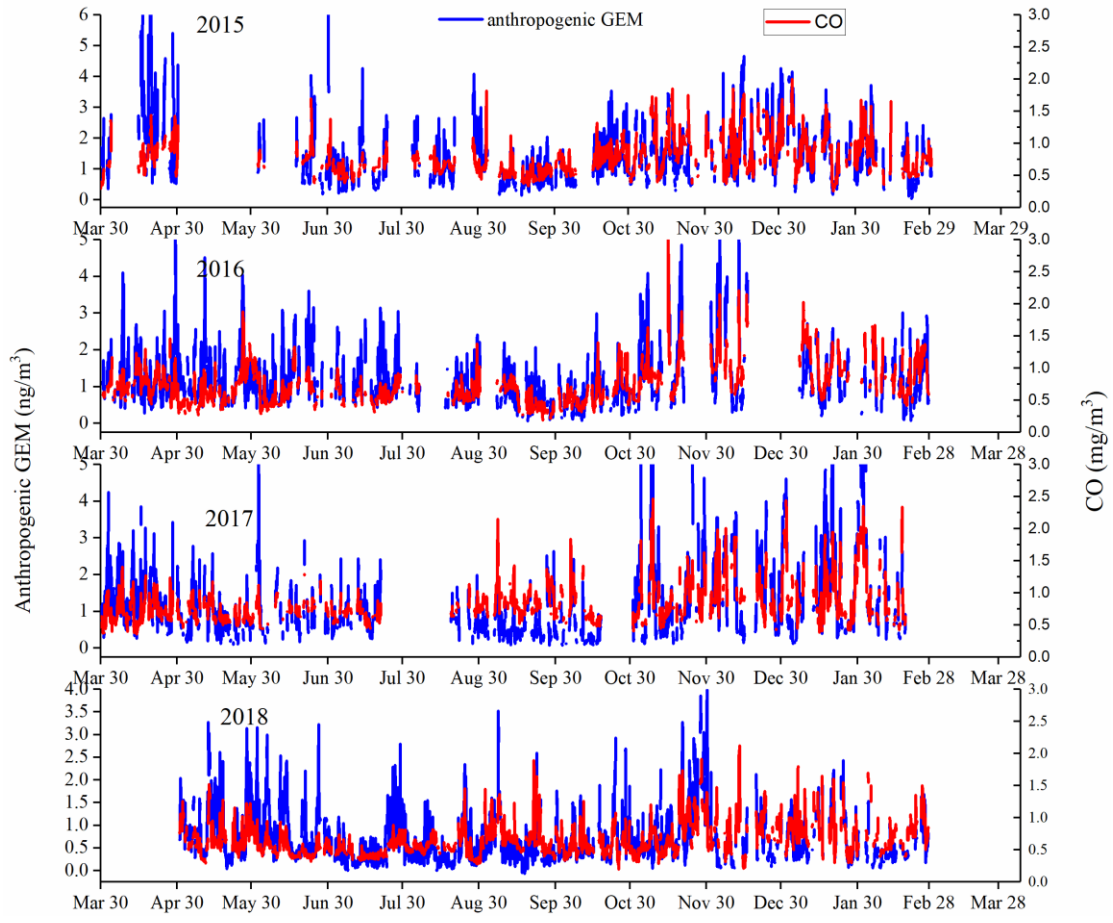
Potential source regions of GEM from shipping activities during 2015 - 2018

As Reviewer#1 also raised similar concerns, we added additional analysis about the verification of PMF results as below.

We verified whether the separation of natural and anthropogenic GEM was credible or not, which is also the main focus of this study. To achieve this, the relationship between particulate black carbon (BC) and GEM concentrations was investigated. On the one hand, BC mainly derives from various combustion processes, which are also the main anthropogenic sources of atmospheric mercury. On the other hand, BC was never introduced into the PMF modeling. As shown in the figure below, the observed total GEM concentrations and BC concentrations only showed weak correlations. This was mainly due to the fact that besides anthropogenic sources, natural sources also contributed significantly to GEM. As a comparison, anthropogenic GEM concentrations (extracted from PMF results) showed much stronger correlations with BC from 2015 to 2018. In addition, the time series of anthropogenic GEM concentrations generally varied consistently with CO (shown in the figure below), which is also a tracer of fuel combustion. This suggests that the PMF results are credible and the separation of anthropogenic and natural GEM has been successfully achieved.

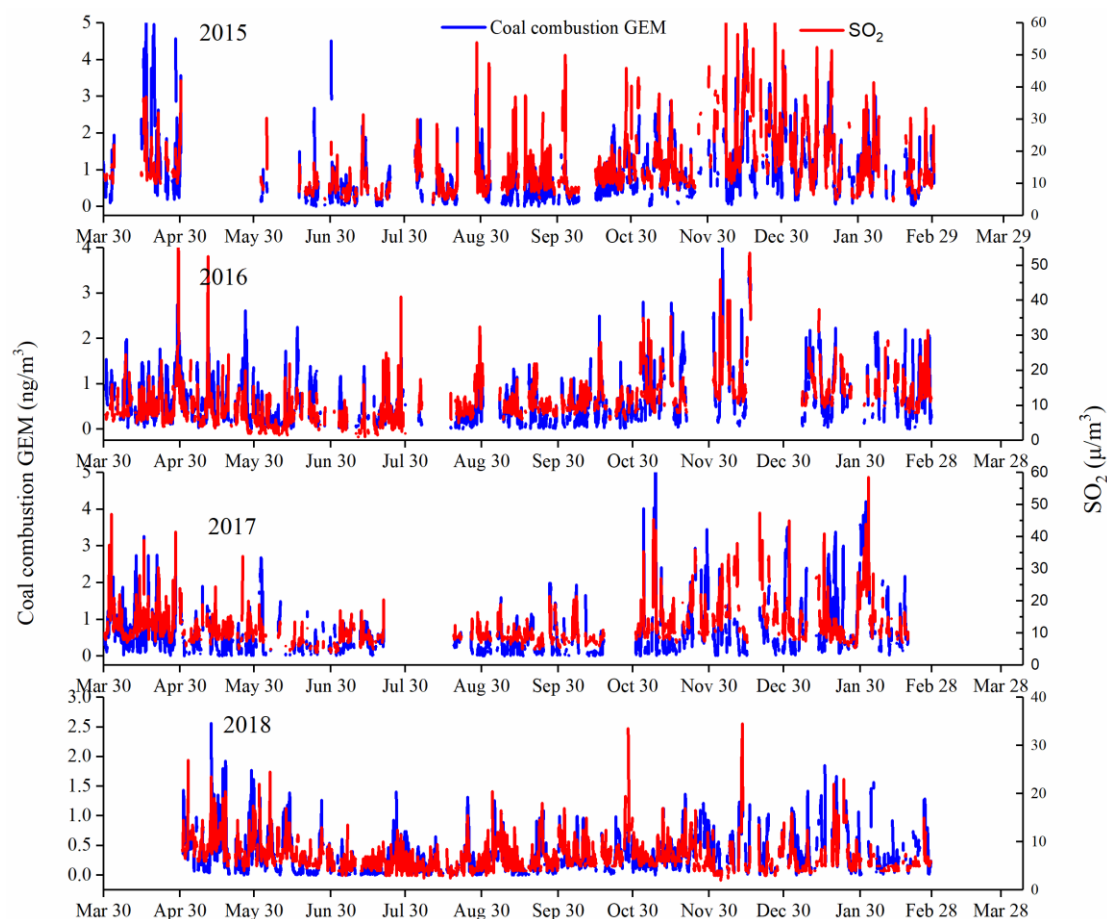


The relationship between observed GEM and BC, anthropogenic GEM (extracted from PMF results) and BC during 2015 – 2018



Time series of anthropogenic GEM and CO concentrations

Furthermore, as shown in the figure below, we examine the time series of coal combustion GEM (extracted from PMF results) and observed SO₂ from 2015 to 2018. It is found that the trend of coal combustion GEM is basically consistent with that of SO₂, which indicates that the coal combustion factor resolved by PMF is credible.



Time series of coal combustion GEM and SO₂ concentrations

In the revised manuscript, we have added a paragraph about the verification of PMF results as below.

“In addition, the relationship between particulate black carbon (BC) and GEM concentration was investigated. On the one hand, BC mainly derived from various combustion processes, which were also the main anthropogenic sources of atmospheric mercury. On the other hand, BC was never introduced into the PMF modeling. As shown in Figure 5, the observed total GEM and BC concentrations only showed weak correlations. This was mainly due to the fact that besides anthropogenic sources, natural sources also contributed significantly to GEM. As a comparison, anthropogenic GEM concentrations (extracted from PMF results) showed much better correlations with BC from 2015 to 2018. In addition, the time-series of anthropogenic

GEM concentrations generally varied consistently with CO, which was also a tracer of fuel combustion (Figure S28). All the evidences above corroborated that by using temperature and NH₃ as tracers for PMF modeling, the separation of anthropogenic and natural GEM can be successfully achieved.

As for the specific anthropogenic mercury sources extracted from PMF results, Figure S29 shows that the time-series of coal combustion GEM also varied consistently with SO₂, indicating that the coal combustion factor resolved by PMF was credible. As shown in Figure S30, the potential source regions of shipping GEM were found mainly over coastal and oceanic areas, indicating the shipping factor resolved in this study was also valid. Figure S31 and Figure S32 show that the PSCF signals of cement production GEM were relatively weak in the YRD region, while there were substantial high PSCF signals for iron and steel production GEM in Eastern China. All the results above collectively confirmed that the PMF results were robust."

5. Lines 47–48: It should be “non-ferrous metal smelters” instead of “non-ferrous smelters”.

Response: The statement “non-ferrous smelters” has been change as “non-ferrous metal smelters” in the revision.

6. Section 2.2: How many valid GEM data were included in the analysis?

Response: The sentence “In this study, the number of valid GEM data was 16266” has been added in the revision.

7. Lines 195–196: This statement is not accurate and lacks evidence. Some of the anthropogenic emission sources vary significantly from season to season. For example, coal combustion for residential use has a much higher level in winter.

Response: Thanks for pointing out this inaccurate statement. the sentence “Considering that seasonal variations of anthropogenic emission are minimum” has been revised as “Considering that the anthropogenic emissions were less temperature dependent, the different seasonal decreasing rates of GEM between the warm and cold seasons should be mostly caused by the seasonal-dependent emission amounts from natural sources” in the revision.

8. Lines 208–209: The p values for all the correlations should be given here.

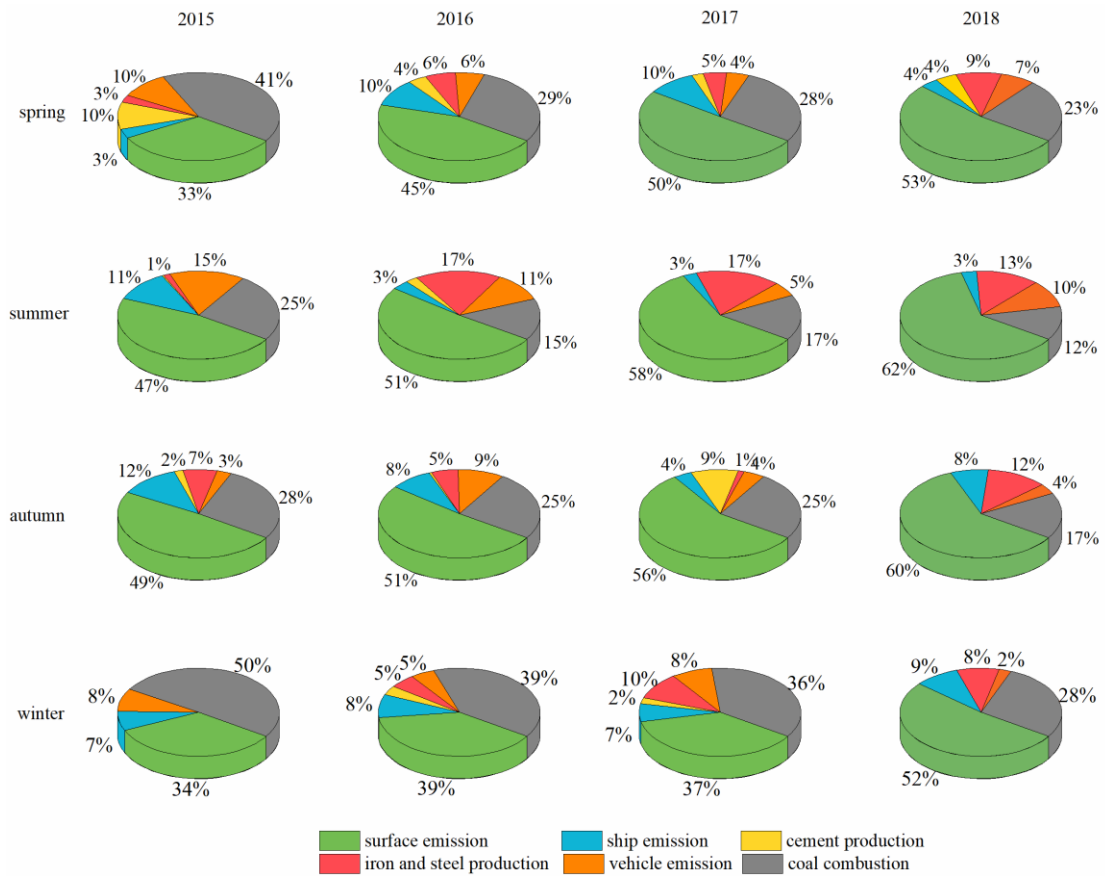
Response: The p values for all the correlations have been added in the revision.

9. Have the authors investigated the correlations between GEM and solar radiation? Solar radiation and temperature could have collinearity to a certain extent. It is possible that the diurnal GEM trend has a more significant correlation with solar radiation. Solar radiation is related to the photoreduction process of Hg in soil, which could be the major natural GEM source in the study area.

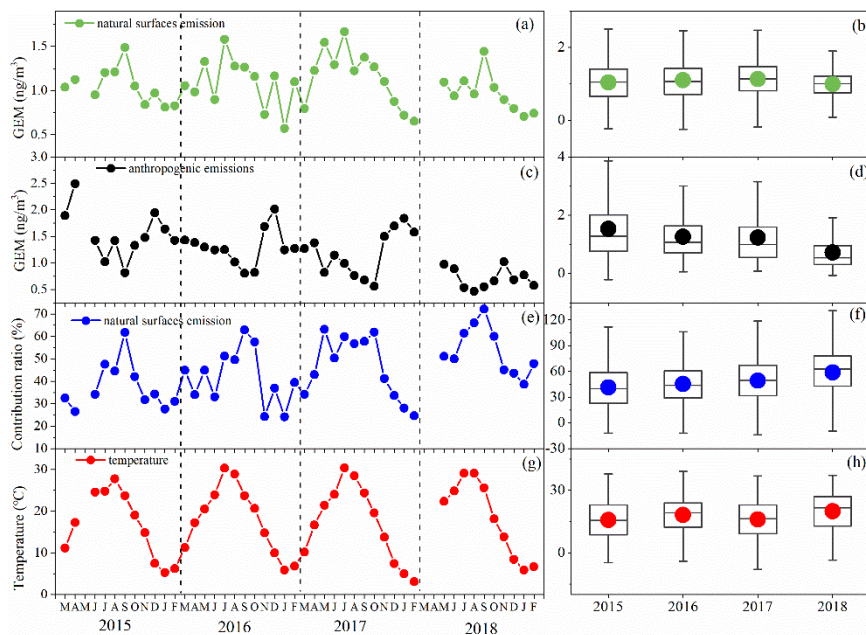
Response: Thanks for this valuable suggestion. We quite agree with the reviewer that solar radiation is a key factor of the photoreduction process of Hg in soil and the diurnal GEM trend likely has a significant correlation with solar radiation. However, due to that solar radiation was not measured in this study, we cannot carry out the corresponding analysis. We will certainly consider the investigation of the relationship between GEM and solar radiation in the future field experiments.

10. Lines 241–245: The choices of NH₃ and O₃ as tracers should be more carefully examined. These two tracers are not directly linked to natural emission sources, but indirectly through temperature. If temperature is already chosen as a tracer for PMF and NH₃ and O₃ are only linked to natural sources through temperature, what is the point of choosing NH₃ and O₃? The authors should pay attention to the other links between NH₃/O₃ and natural sources. Say the links through solar radiation, land surface type, and so on. Moreover, the PMF method usually chooses primary air pollutants as tracers, e.g., VOC species profiles, ions on particles, heavy metal profiles, etc. Secondary air pollutants, such as O₃, are usually avoided to be used as a tracer for PMF, because all the coefficients resulting from the PMF model need to be positive while it is not always the case for secondary air pollutants like O₃, not to mention that O₃ and GEM are potentially not independent variables. O₃ might act as an oxidizer for GEM under certain conditions (e.g., high humidity), although this mechanism is not clear so far. Therefore, the authors should either remove O₃ as a tracer or explain why in this case O₃ is applicable from PMF.

Response: After considering the reviewer's insightful suggestion, we agree that O₃ is not suitable as the tracer of natural emission and shouldn't be used as a tracer for PMF modeling. Hence, we have removed O₃ and re-run the PMF model for the whole multi-year dataset. The new modeling results are shown in the following figures. We found that after the removal of O₃, the contributions of natural and anthropogenic sources to GEM from 2015 to 2018 didn't change much, hence the major conclusion hasn't been affected. In general, the contributions of natural sources to GEM increased slightly. For example, before removing O₃, the relative contribution of natural surface emissions to GEM increase from 36% in 2015 to 53% in 2018. After removing O₃, its contribution increases from 41% in 2015 to 57% in 2018. In the revision, we replace Figure 5 and Figure 6 with the following two figures, and modified the corresponding specific contribution values.



Contributions of natural surface emissions and anthropogenic sources to atmospheric GEM in the four seasons during 2015 – 2018.



The monthly and annual GEM concentrations contributed by natural surface emissions (a-b) and anthropogenic emissions (c-d) from 2015 to 2018. (e-f) The monthly and annual contribution of natural surface emissions to GEM concentrations from 2015 to 2018. (g-h) The corresponding ambient temperature from 2015 to 2018.

References:

- Fan, Q., Zhang, Y., Ma, W., Ma, H., Feng, J., Yu, Q., Yang, X., Ng, S. K. W., Fu, Q., and Chen, L.: Spatial and Seasonal Dynamics of Ship Emissions over the Yangtze River Delta and East China Sea and Their Potential Environmental Influence, *Environmental science & technology*, 50, 1322-1329, 10.1021/acs.est.5b03965, 2016.
- Liu, K., Wu, Q., Wang, L., Wang, S., Liu, T., Ding, D., Tang, Y., Li, G., Tian, H., Duan, L., Wang, X., Fu, X., Feng, X., and Hao, J.: Measure-Specific Effectiveness of Air Pollution Control on China's Atmospheric Mercury Concentration and Deposition during 2013-2017, *Environmental science & technology*, 10.1021/acs.est.9b02428, 2019.
- Liu, Z., Lu, X., Feng, J., Fan, Q., Zhang, Y., and Yang, X.: Influence of Ship Emissions on Urban Air Quality: A Comprehensive Study Using Highly Time-Resolved Online Measurements and Numerical Simulation in Shanghai, *Environmental science & technology*, 51, 202-211, 10.1021/acs.est.6b03834, 2017.
- Tang, Y., Wang, S. X., Wu, Q. R., Liu, K. Y., Wang, L., Li, S., Gao, W., Zhang, L., Zheng, H. T., Li, Z. J., and Hao, J. M.: Recent decrease trend of atmospheric mercury concentrations in East China: the influence of anthropogenic emissions, *Atmospheric Chemistry and Physics*, 18, 8279-8291, 10.5194/acp-18-8279-2018, 2018.
- Zhu, W., Lin, C.-J., Wang, X., Sommar, J., Fu, X., and Feng, X.: Global observations and modeling of atmosphere-surface exchange of elemental mercury: a critical review, *Atmospheric Chemistry and Physics*, 16, 4451-4480, 10.5194/acp-16-4451-2016, 2016.

1 Assessing contributions of natural surface and anthropogenic emissions to
2 atmospheric mercury in a fast developing region of Eastern China from
3 2015 to 2018

4 Xiaofei Qin¹, Leiming Zhang², Guochen Wang¹, Xiaohao Wang³, Qingyan Fu^{3,4}, Jian Xu¹, Hao Li¹,
5 Jia Chen¹, Qianbiao Zhao^{3,4}, Yanfen Lin^{3,4}, Juntao Huo^{3,4}, Fengwen Wang^{5,4}, Kan Huang^{1,5,6,7*},
6 Congrui Deng^{1,*}

8 ¹Center for Atmospheric Chemistry Study, Shanghai Key Laboratory of Atmospheric Particle
9 Pollution and Prevention (LAP3), Department of Environmental Science and Engineering, Fudan
10 University, Shanghai, 200433, China

11 ²Air Quality Research Division, Science and Technology Branch, Environment and Climate Change
12 Canada, Toronto, M3H 5T4, Canada

13 ³Shanghai Environmental Monitoring Center, Shanghai, 200030, China

14 ⁴[State Ecologic Environmental Scientific Observation and Research Station for Dianshan Lake,
15 Shanghai 201713, China](#)

16 ⁵State Key Laboratory of Coal Mine Disaster Dynamics and Control, College of Environment and
17 Ecology, Chongqing University, Chongqing 400030, China

18 ⁶Institute of Eco-Chongming (IEC), Shanghai, 202162, China

19 ⁷Institute of Atmospheric Sciences, Fudan University, Shanghai 200433, China

Formatted: Superscript

20
21 **Abstract**

22 Mercury (Hg) is a global toxic pollutant that can be released into the atmosphere through
23 anthropogenic and natural sources. The uncertainties in the estimated emission amounts are much
24 larger from natural than anthropogenic sources. A method was developed in the present study to
25 quantify the contributions of natural surface mercury emissions to ambient gaseous elemental
26 mercury (GEM) concentrations through application of positive matrix factorization (PMF) analysis
27 with temperature, O_3 , and NH_3 as indicators of GEM emissions from natural surfaces. GEM
28 concentrations were continuously monitored at a 2-hourly resolution at a regional background site
29 in the Yangtze River Delta in Eastern China during 2015-2018. Annual average GEM concentrations
30 were in the range of 2.03-3.01 ng/m^3 , with a strong decreasing trend at a rate of $-0.32 \pm 0.07 \text{ ng m}^{-3}$
31 yr^{-1} from 2015 to 2018, which was mostly caused by reduced anthropogenic emissions since 2013.
32 The estimated contributions from natural surface emissions of mercury to the ambient GEM
33 concentrations were in the range of ~~1.00-1.13~~~~0.90-1.01~~ ng/m^3 on annual average with insignificant
34 interannual changes, but the relative contribution increased significantly from ~~36~~~~41~~% in 2015 to
35 ~~53~~~~57~~% in 2018, gradually surpassing those from anthropogenic sources.

36

37 1. Introduction

38 Mercury has long been recognized as a toxic pollutant due to its bioaccumulation and health
39 effects (Driscoll et al., 2013b;Clarkson and Magos, 2006;Schroeder and Munthe, 1998;Horowitz et
40 al., 2017;Fu et al., 2012;Wright et al., 2018). Mercury in the atmosphere can be transported globally,
41 mostly in the form of gaseous elemental mercury (GEM) due to its long lifetime in air (Driscoll et
42 al., 2013a). Clarifying sources and quantifying emissions from the major sources of atmospheric
43 mercury are critical for understanding the biogeochemical cycle of mercury and developing mercury
44 reduction strategies. Mercury in the atmosphere is released from both natural and anthropogenic
45 sources. Natural sources include volcanoes, geological weathering, forest fires, re-emissions of pre-
46 deposited mercury from natural surfaces, etc (Gustin et al., 2008;Mason and Sheu, 2002). Among
47 these sources, emissions from natural surfaces are the major ones and a number of studies have been
48 devoted to understanding the processes of natural surface emissions (Xu et al., 1999;Lindberg et al.,
49 2002;Kocman et al., 2013). Anthropogenic sources mainly include coal-fired power plants, non-
50 ferrous metal smelters, and waste incineration (Friedli et al., 2009). Globally, natural sources
51 released about 5200 tons mercury into the atmosphere on an annual basis, which contributed up to
52 two-thirds of the global atmospheric mercury budget, while those by anthropogenic sources was
53 estimated to be around 2300 tons (Pirrone et al., 2010). In China, the total mercury emissions
54 released from natural and anthropogenic sources were estimated to be 574.5 ton yr⁻¹, and 571 ton
55 yr⁻¹, respectively (Wang et al., 2016;Zhang et al., 2015).

56 During the past decades, anthropogenic emissions of mercury in Europe and North America
57 have been reduced significantly through phasing out mercury from many commercial products as
58 well as benefiting from SO₂ and NO_x emission reduction from coal-fired utilities, resulting in
59 considerable decrease in atmospheric mercury concentrations in these regions (e.g., approximately
60 1-2% yr⁻¹ decrease from 1990 to 2013) (Streets et al., 2011;Zhang et al., 2016). In China,
61 anthropogenic mercury emissions decreased from 571 ton in 2013 to 444 ton in 2017 due to the co-
62 benefits of aggressive air pollutant control measures implemented in this period (Liu et al., 2019a).
63 GEM concentrations measured at a rural site north of Shanghai showed a substantially decreasing
64 trend from 2014 to 2016 (Tang et al., 2018).

65 With the decrease of anthropogenic mercury emissions in many parts of the world (Zhang et
66 al., 2016), the contributions of natural emissions to total mercury budget are expected to be more

67 important. However, the trends of natural emissions are still unclear due to the difficulties in directly
68 measuring GEM emissions from natural surfaces (Zhu et al., 2015). Existing estimates of GEM
69 emission from natural sources have large uncertainties (e.g., from 1500 to 5207 Mg yr⁻¹ on global
70 scale), limiting our understanding of the role of natural emissions in the global mercury cycle (Song
71 et al., 2015; Wang et al., 2014b). For example, a study at rural Beijing showed that modeled GEM
72 concentrations were underestimated by about 40% than measurements from April to September
73 2009 due to the absence of natural emission inventories (Wang et al., 2014a). Hence, it is meaningful
74 to develop a method to quantify the contributions of natural surface emissions to total mercury
75 budget in the atmosphere, especially in China where anthropogenic emissions have been fast
76 decreasing in recent years.

77 The purpose of the present study is to differentiate the contributions of natural surface
78 emissions and anthropogenic emissions to the measured ambient GEM concentrations collected
79 during a four-year period at a regional background site in the Yangtze River Delta (YRD) of Eastern
80 China. This was done by conducting positive matrix factorization (PMF) analysis with identified
81 variables as tracers of natural surface mercury emissions. Results presented in this study provide an
82 approach that can be potentially used for improving mercury emission databases for natural sources.

83

84 **2. Materials and methods**

85 **2.1 Site description**

86 Shanghai, situated in the YRD region, is one of the most developed cities in China. Like in
87 many other cities in China, severe air pollutions have occurred frequently in this city in the past
88 decades. A supersite has been set up next to the Dianshan Lake in Qingpu District of rural Shanghai
89 (Figure 1) as part of the framework of State Environmental Protection Scientific Observation and
90 Research Station. This supersite is designed to represent the regional scale air pollution
91 characteristics in the YRD region based on the following two considerations: (1) it is located in the
92 conjunction area of Shanghai, Jiangsu, and Zhejiang provinces; and (2) there are no large point
93 sources such as coal-fired power plants, nonferrous metal smelting, and cement production within
94 20km distance surrounding the site. This site was established in 2013 and its capacity has been
95 gradually built by measuring a set of atmospheric parameters, including meteorological factors,
96 trace gases, aerosol physical and chemical parameters, vertical profiles of ozone and particles, etc.

97 More detailed descriptions of the site can be found elsewhere (Qin et al., 2019;Duan et al., 2017).

98

99 **2.2 Measurements of gaseous elemental mercury**

100 An automated mercury vapor analyzer Tekran 2537B/1130/1135 was installed on the third floor
101 of a building for real time continuous GEM measurements since January 2015. GEM was measured
102 based on the principle of cold vapor atomic fluorescence spectroscopy (CVAFS) (Landis and Keeler,
103 2002). Briefly, ambient GEM was collected on gold traps and then thermally decomposed to GEM
104 before detection. The sampling interval of GEM was 5 minutes with a flow rate of 1L/min. More
105 details of this instrument can be found elsewhere (Mao et al., 2008).

106 Strict quality control procedures were followed during the sampling process. Denuders and
107 quartz filters were prepared and cleaned according to the instructions in Tekran technical notes
108 before sampling. Routine calibration with internal permeation source was performed every 47 hours
109 and manual injections of standard saturated mercury vapor were conducted to ensure the accuracy
110 of these automated calibrations. The KCl-coated denuder, Teflon-coated glass inlet, and impactor
111 plate were replaced weekly and quartz filters were replaced monthly. Individual extremely high
112 GEM concentrations that occasionally happened were regarded as outliers and were excluded from
113 the data analysis. In this study, the number of valid GEM data was 16266.

114

115 **2.3 Measurements of other air pollutants and meteorological parameters**

116 Water soluble ions in PM_{2.5} and soluble gases were continuously measured by Monitor for
117 Aerosols and Gases in ambient Air (MARGA) operated at a flow rate of 16.7 L/min with a time
118 resolution of one hour, as detailed in (Chang et al., 2016). Briefly, water-soluble gases in the airflow
119 were removed by an absorbing liquid, then the particles were induced by a supersaturation of water
120 vapor to grow into droplets before they were collected and transported into the analytical chamber.

121 Trace metals in PM_{2.5} were continuously measured by using the Xact 625 ambient metals
122 monitor (Cooper Environmental, Beaverton, OR, USA) operated at a flow rate of 16.7 L/min with
123 hourly resolution, as detailed in (Yu et al., 2019). Briefly, the particles in the airflow were deposited
124 onto a Teflon filter tape, and then transported into the spectrometer where the particles were
125 analyzed with an X-ray fluorescence. Black carbon in PM_{2.5} was measured by a multiwavelength
126 Aethalometer (AE-33, Magee Scientific). Ambient particles were collected on a paper tape at a flow

Formatted: Font: 10.5 pt

Formatted: Font: 10.5 pt

Formatted: Font: 10.5 pt

Formatted: Font: 10.5 pt

Formatted: Font: 10.5 pt

Formatted: Font: 10.5 pt

Formatted: Font: 10.5 pt

Formatted: Font: 10.5 pt

Formatted: Font: 10.5 pt

127 rate of 5 L/min. Aerosol light absorptions of BC were measured at seven wavelengths of 370, 470,
128 520, 590, 660, 880, and 950nm.

129 ~~Ozone~~ Sulfur dioxide, carbon monoxide, and PM_{2.5} were measured by Thermo Fisher 439i,
130 Thermo Fisher 48i-TLE, and Thermo Fisher 1405-F, respectively. Meteorological parameters
131 including ambient temperature, wind speed, and wind direction were obtained at the sampling site
132 by using the automatic weather station (AWS). Bivariate polar plots (BPP) were applied in this study
133 to explore how GEM concentrations change with different wind direction and wind speed, which
134 has proven to be a reliable method for identifying different source regions (Carslaw et al.,
135 2006; Carslaw and Ropkins, 2012; Chang et al., 2017). Here, the open-source software “openair” in
136 R was used to create BPPs (Carslaw and Ropkins, 2012).

137

138 2.4 Positive matrix factorization (PMF)

139 The PMF model has been proven to be a useful tool to provide quantitative source profiles and
140 source contributions (Xu et al., 2017; Gibson et al., 2015). The basic principle of PMF is that
141 concentrations of the samples were determined by the source profiles with different contributions,
142 which can be described as follows:

$$143 X_{ij} = \sum_{k=1}^P g_{ik} f_{kj} + e_{ij} \quad (1)$$

144 where X_{ij} represents the concentration of the j th species in the i th sample, g_{ik} is the contribution
145 of the k th factor in the i th sample, f_{kj} provides the information of the mass fraction of the j th
146 species in the k th factor, e_{ij} is the residual for specific measurement, and P represents the number
147 of factors.

148 The objective function expressed in Eq. (2) below, which is the sum of the square of the
149 difference between the measured and modeled concentrations weighted by the concentration
150 uncertainties, needs to be minimized before the PMF model determines the optimal non-negative
151 factor profiles and contributions. (Cheng et al., 2015)

$$152 Q = \sum_{i=1}^n \sum_{j=1}^m \left(\frac{X_{ij} - \sum_{k=1}^P A_{ik} F_{kj}}{S_{ij}} \right)^2 \quad (2)$$

153 where X_{ij} represents the concentration of the j th contamination in the i th sample, m is the total
154 number of pollutant, and n is the total number of sample. A_{ik} represents the contribution of the k th
155 factor on the i th sample and F_{kj} represents the mass fraction of the j th pollutant in the k th factor.
156 S_{ij} is the uncertainty of the j th pollutant on the i th factor and P is the number of factors. In this

157 study, we explored the number of factors from three to eight with the optimal solutions determined
158 by the slope of the Q value versus the number of factors. For each run, the stability and reliability
159 of the outputs were assessed by referring to the Q value, residual analysis, and correlation
160 coefficients between observed and predicted concentrations. Finally, we found that a six-factor
161 solution showed the most stable results and gave the most reasonable interpretation. A dataset
162 containing uncertainty values of each species was created and digested into the model, with the error
163 fraction being assumed to be 15% for GEM concentration and 10% for other compounds (Xu et al.,
164 2017;Polissar et al., 1998).

165 It should be noted that Fpeak model run at the strength of 0.5 was done by using the rotation
166 tools in PMF and the results were summarized in Table S1. For all seasons, the increase of the Q-
167 value due to the Fpeak rotation with a dQ was less than 1% of the Base Run Q (robust) value.
168 According to the User Guide of PMF5.0, it was acceptable when the %dQ was less than 5%. The
169 profiles and contributions of each source were examined and there were no significant differences
170 between the factor contributions of Base Run and rotation results. Hence, the Base Run results were
171 used in this study.

172

173 **2.5 Annual changes of anthropogenic mercury emission in China and YRD**

174 It was reported that the annual anthropogenic atmospheric mercury emission in China
175 significantly increased from 147 tons in 1978 to 549 tons in 2010 (Wu et al., 2016). In more recent
176 years, in order to cope with the severe air pollution situation, the Chinese government has taken
177 many rigorous and ambitious measures such as introduction of ultra-low emissions standards on
178 power plants and phasing out of small factories with high-emissions (Zheng et al., 2018). As a result,
179 mercury emissions from anthropogenic sources have since been declining in China. For the five-
180 year period of 2013-2017, annual total anthropogenic mercury emissions in China were estimated
181 to be 571, 547, 528, 486, and 444 tons, respectively, or a total decline of 127 tons. During the same
182 period, the reduction of anthropogenic mercury emissions reached 60 tons in eastern China (Liu et
183 al., 2019a).

184

185 **3. Results and Discussion**

186 **3.1 The measured gaseous elemental mercury**

187 **3.1.1 Decreasing trend of gaseous elemental mercury**

188 The measured annual mean GEM concentrations were 3.01 ± 1.03 , 2.58 ± 0.84 , 2.52 ± 0.84 ,
189 and 2.03 ± 0.69 ng/m³ from 2015 to 2018. By using the Theil-Sen function, monthly GEM exhibited
190 a significantly decreasing trend from 2015 to 2018 ($p < 0.05$) with a rate of -0.32 ± 0.07 ng m⁻³ yr⁻¹
191 (Figure 2a). This decreasing trend was consistent with the trends of mass concentrations of PM_{2.5}
192 and SO₂ (Figure 2b & 2c), which were attributed to the implementation of the Clean Air Action
193 since 2013 in China (Zheng et al., 2018). As mentioned earlier (Section 2.5), the nationwide
194 reduction of anthropogenic mercury emissions should be largely responsible for the significant
195 decrease in GEM concentration observed at the YRD regional background site.

196 Seasonal average GEM concentrations decreased from 3.62 ng/m³ to 2.17 ng/m³ with a rate of
197 -0.37 ng m⁻³ yr⁻¹ in spring, from 2.89 ng/m³ to 1.98 ng/m³ with a rate of -0.26 ng m⁻³ yr⁻¹ in summer,
198 from 2.62 ng/m³ to 1.94 ng/m³ with a rate of -0.22 ng m⁻³ yr⁻¹ in autumn, and from 2.91 ng/m³ to
199 1.82 ng/m³ with a rate of -0.35 ng m⁻³ yr⁻¹ in winter (Figure 3). The decreasing rates of GEM were
200 ~30% lower in the warm seasons than the cold seasons. Considering that seasonal variations of
201 anthropogenic emission were less temperature dependent~~are minimum~~, the different seasonal
202 decreasing rates of GEM between the warm and cold seasons should be mostly caused by the
203 seasonal-dependent emission amounts from natural sources, knowing that natural emissions are
204 controlled by solar radiation and temperature, among other factors (Howard and Edwards,
205 2018;Pannu et al., 2014;Mason, 2009).

206

207 **3.1.2 Impact of temperature on ambient gaseous elemental mercury**

208 In a previous study we showed that GEM concentrations tended to rise with increasing
209 temperature in the YRD region, which was considered to be the effect of temperature-dependent
210 emission amounts from natural surfaces (Qin et al., 2019). Here, to qualitatively investigate the role
211 of natural surface emissions on ambient GEM concentration, diurnal profiles of the bi-hourly GEM
212 concentration and temperature are exhibited in Figure 4. If looking at the whole year data together,
213 moderate to high correlations were seen between the diurnal variations of GEM and temperature in
214 2016, 2017, and 2018 with R² being 0.30 to 0.86 ($p < 0.05$), except in 2015 with little correlation
215 with R² being only 0.03 ($p > 0.05$) (Figure 4a-4d). The maximum GEM concentrations generally
216 appeared around 10AM - 14PM, mostly coincided with daily peak temperature. These findings

Formatted: Font color: Auto

217 provided strong evidence of temperature-dependent GEM sources.

218 Due to the large differences in ambient temperature between warm (from June to November)
219 and cold (from December to May) seasons in the YRD region, the effects of temperature-dependent
220 GEM sources on the ambient GEM concentrations should be different in different seasons. As
221 expected, high correlations between GEM concentrations and temperature were found in the warm
222 seasons with R^2 being in the range of 0.15 to 0.87 (Figures 4e-4h), while nearly no correlations in
223 the cold seasons (Figures 4i-4l). Thus, the influence of natural surface emissions on ambient GEM
224 concentration was important in the warm seasons, but may not be the case in the cold seasons. The
225 seasonal bivariate polar plots of GEM showed that high GEM concentrations were associated
226 frequently with air flows from the south and southwest and occasionally with those from the north,
227 particularly in summer (Figure S1). This was consistent with the findings in previous studies which
228 showed stronger natural surface emissions in South and Southwest China than North China (Wang
229 et al., 2016;Feng et al., 2005;Wang et al., 2006;Sommar et al., 2016). Hence, in the context of
230 significant reduction of anthropogenic mercury emission in China, especially in North China (Liu
231 et al., 2019b), natural surface emissions significantly impacted the ambient GEM concentrations at
232 this sampling site.

233

234 **3.2 Quantify the contributions from natural surface emissions to ambient gaseous elemental** 235 **mercury**

236 **3.2.1 Development of the approach**

237 A method is developed below for quantifying the contributions of GEM emissions from natural
238 surfaces to ambient GEM concentrations through application of the PMF model by introducing
239 specific variables related to natural surface emissions as traces. The first step is to identify what
240 variables are directly or indirectly related to the natural surface emissions of GEM. Temperature is
241 certainly a dominant one as has been demonstrated in existing soil-air fluxes studies of mercury
242 (Wang et al., 2014b;Zhu et al., 2016;Poissant and Casimir, 1998). The formation pathways of Hg^0
243 in soil are all related to temperature, an empirical rule suggests that a $10^\circ C$ temperature increase
244 doubles the rates for chemical reaction near room temperature, which has been proven to be
245 applicable to Hg^{II} reduction in boreal soil (Moore and Carpi, 2005;Quinones and Anthony,
246 2011;Wang et al., 2016;Pannu et al., 2014). Discussions in Section 3.1.2 also suggested temperature

247 as a potentially useful tracer for predicting natural surface emissions of GEM. A second candidate
248 of tracers could be ambient NH₃ concentration because soil emissions of GEM and NH₃, both of
249 which are temperature-dependent, are treated in a similar way in air-quality modeling studies
250 (Wright and Zhang, 2015;Zhang et al., 2010). ~~The third potential tracer could be O₃ concentration~~
251 ~~because high temperature can promote the formation of O₃ (Kerr et al., 2019;Kerr and Waugh,~~
252 ~~2018;Schnell and Prather, 2017).~~As shown in Figure S2, the mean diurnal variations of GEM
253 concentrations highly correlated with ambient temperature as well as NH₃~~and O₃ concentrations.~~
254 From this perspective, NH₃~~and O₃~~ can be regarded as ~~an~~ indirect proxy~~ies~~ for the natural surface
255 emissions of GEM. In a previous study, we have applied principal component analysis for source
256 apportionment of mercury in this area, and the source factor with high loadings for temperature ~~and,~~
257 NH₃~~and O₃~~ was interpreted as natural surface emissions of GEM (Qin et al., 2019).

258 Hence, in this study, we included the data of temperature; ~~and~~ NH₃~~and O₃~~ into the PMF model
259 to apportion the sources of GEM. As shown in Figures S3-S18, the source apportionment results for
260 all the seasons of 2015-2018 all resolved a similar factor with high loadings of temperature ~~and O₃~~
261 and moderate loadings of NH₃ and GEM. This factor was thought to be the natural surface emission
262 sources of mercury. As for the other resolved factors, ~~the factor with high loadings of V and Ni~~
263 ~~evidently represented shipping emissions, because Ni and V have been considered as typical tracers~~
264 ~~of heavy oil combustion which has been commonly used in marine vessels (Viana et al., 2009). The~~
265 ~~factor with high loading of Ca was assigned to cement production as the raw materials used in~~
266 ~~cement production contain a large amount of calcium compounds. Moderate loadings of multiple~~
267 ~~species including Cr, Mn, and Fe were found in one factor which was identified as iron and steel~~
268 ~~production. The factor with high loading of NO was identified as vehicle emissions, as the major~~
269 ~~source of NOx in the YRD region is mobile oil combustion (Tang et al., 2018). And the last factor~~
270 ~~was identified as coal combustion due to the high loadings of As and Se, and moderate contributions~~
271 ~~from Pb and SO₄²⁻. As, Se, and Pb were all typical tracers of coal combustion and the precursor of~~
272 ~~SO₄²⁻ (i.e. SO₂) also mainly derived from coal combustion. ~~the factor with high loadings of V and~~~~
273 ~~Ni evidently represented shipping emissions. The factor with high loadings of Ca was assigned to~~
274 ~~cement production. Moderate loadings of multiple species including Cr, Mn, and Fe was found in~~
275 ~~one factor which were identified as iron and steel production. The factor with high loadings of NO~~
276 ~~was identified as vehicle emissions. And the last factor was identified as coal combustion due to the~~

Field Code Changed

Field Code Changed

Field Code Changed

Field Code Changed

277 ~~high loadings of As and Se, and moderate contributions of Pb and SO₄²⁻.~~

278 In order to verify the PMF modeling results, we first examined the PMF model performance.
279 Table S2 shows the coefficient of determination (R²) for GEM according to the observation-
280 prediction scatter plots (Figure S20-S23). The R² values ranged from 0.37 to 0.89, suggesting an
281 acceptable model performance. Figure S24-S27 display the time series of observed and predicted
282 GEM concentrations from 2015-2018, which revealed that, except for a few extremely high
283 observation values, the model can relatively well reproduce the observed GEM concentration on an
284 hourly basis.

285 To further verify the reliability of the resolved factors, the correlations between the mass
286 contributions of all factors to GEM and temperature were examined on the basis of diurnal profiles.
287 As shown in Figure S19, positive correlation was only found between the natural surface emission
288 factor and temperature while the other resolved factors (i.e. vehicle emission, coal combustion,
289 shipping activities, cement production, and iron and steel production) did not show this relationship.

290 ~~This further corroborated that by using temperature, NH₃, and O₃ as tracers, the natural surface
291 emissions of GEM can be identified and quantified.—~~

292 ~~In addition, the relationship between particulate black carbon (BC) and GEM concentration was
293 investigated. On the one hand, BC mainly derived from various combustion processes, which were
294 also the main anthropogenic sources of atmospheric mercury. On the other hand, BC was never
295 introduced into the PMF modeling. As shown in Figure 5, the observed total GEM and BC
296 concentrations only showed weak correlations. This was mainly due to the fact that besides
297 anthropogenic sources, natural sources also contributed significantly to GEM. As a comparison,
298 anthropogenic GEM concentrations (extracted from PMF results) showed much better correlations
299 with BC from 2015 to 2018. In addition, the time-series of anthropogenic GEM concentrations
300 generally varied consistently with CO, which was also a tracer of fuel combustion (Figure S28). All
301 the evidences above corroborated that by using temperature and NH₃ as tracers for PMF modeling,
302 the separation of anthropogenic and natural GEM can be successfully achieved.~~

303 ~~As for the specific anthropogenic mercury sources extracted from PMF results, Figure S29
304 shows that the time-series of coal combustion GEM also varied consistently with SO₂, indicating
305 that the coal combustion factor resolved by PMF was credible. As shown in Figure S30, the potential
306 source regions of shipping GEM were found mainly over coastal and oceanic areas, indicating the~~

Formatted: Indent: First line: 0 ch

Formatted: Indent: First line: 2 ch

Formatted: Subscript

307 shipping factor resolved in this study was also valid. Figure S31 and Figure S32 show that the PSCF
308 signals of cement production GEM were relatively weak in the YRD region, while there were
309 substantial high PSCF signals for iron and steel production GEM in Eastern China. All the results
310 above collectively confirmed that the PMF results were robust.

311 **3.2.2 Increasing contributions from natural surface emissions to ambient gaseous elemental** 312 **mercury**

313 Figure 65 summarizes the contributions of natural surface emissions and anthropogenic
314 emissions to GEM on seasonal basis from 2015 – 2018. The contributions of natural surface
315 emissions to GEM were ~40% higher in summer ($1.15 \pm 0.60 \text{ ng/m}^3$ ~~$1.09 \pm 0.58 \text{ ng/m}^3$~~) than winter
316 ($0.82 \pm 0.57 \text{ ng/m}^3$ ~~$0.78 \pm 0.54 \text{ ng/m}^3$~~). Besides, the contributions of natural surface emissions to GEM
317 exhibited an upward trend, e.g., increased from ~~33% to 53%~~ ~~32% to 52%~~ in spring, ~~47% to 62%~~ ~~39%~~
318 ~~to 63%~~ in summer, ~~49% to 60%~~ ~~41% to 53%~~ in autumn, and ~~34% to 52%~~ ~~32% to 43%~~ in winter, from
319 2015-2018 (Figure 65). In contrast, the contributions from anthropogenic sources to GEM showed
320 a downward trend, of which the decreased contribution from coal combustion accounted the most.
321 Coal combustion has been widely regarded as the dominant anthropogenic source of mercury
322 emissions at the global scale, and China is known as the largest coal producer and consumer in the
323 world (Zhang et al., 2012; Wu et al., 2006). Since 2013, a series of key air pollution control measures
324 have been applied in China to reduce the emission of air pollutants (Zheng et al., 2018). YRD regions
325 also took actions by regulating on the amount of coal consumption, promoting renewable energy
326 development and so on (Zheng et al., 2016). Hence, the decreased contribution of coal combustion
327 was attributed to the implementation of aggressive air pollutant control measures in China in recent
328 years, which subsequently led to an increase in the relative contribution of natural surface emissions
329 to GEM.

330 The absolute GEM concentrations contributed by both natural surface emissions and
331 anthropogenic emissions can be extracted from the PMF modeling results. Figure 76 exhibits the
332 monthly and yearly profiles from 2015 to 2018. Strong seasonal cycles of GEM contributed by
333 natural surface emissions were seen, corresponding to the seasonal pattern of ambient temperature
334 (Figure 76g) and the simulated monthly Hg fluxes from natural surface emissions in China (Wang
335 et al., 2016). The annual GEM concentration contributed by natural surface emissions was estimated
336 to be $1.04 \pm 0.55 \text{ ng/m}^3$, $1.10 \pm 0.56 \text{ ng/m}^3$, $1.13 \pm 0.56 \text{ ng/m}^3$, and $1.00 \pm 0.45 \text{ ng/m}^3$ ~~$0.94 \pm 0.57 \text{ ng/m}^3$~~ ;

337 $1.01 \pm 0.63 \text{ ng/m}^3$, $1.00 \pm 0.62 \text{ ng/m}^3$, and $0.90 \pm 0.48 \text{ ng/m}^3$ from 2015 to 2018, respectively (Figure
338 76a & 76b), which almost remained unchanged. This could be mainly explained by the little
339 variation of annual temperature (Fig. 76h) and wind pattern from 2015 to 2018 (Fig. S28S33). On
340 the contrary, the annual GEM concentration contributed by anthropogenic emissions was estimated
341 to be $1.53 \pm 1.04 \text{ ng/m}^3$, $1.26 \pm 0.78 \text{ ng/m}^3$, $1.23 \pm 0.95 \text{ ng/m}^3$, and $0.82 \pm 0.58 \text{ ng/m}^3$; $1.67 \pm 1.06 \text{ ng/m}^3$;
342 $1.51 \pm 0.77 \text{ ng/m}^3$, $1.38 \pm 1.02 \text{ ng/m}^3$, and $0.80 \pm 0.63 \text{ ng/m}^3$ from 2015 to 2018, respectively, showing
343 an obvious decreasing trend (Figure 76c & 76d). It was noted that the GEM concentration
344 contributed by anthropogenic emissions dropped the most from 2017 to 2018 with a rate of around
345 40%. By referring to the Table S3, SO₂ and CO also decreased significantly of about 35% and 18%.
346 As SO₂ and CO were the main primary gaseous pollutants emitted from fuel combustions, their
347 sharp decreases indicated the significant reduction of anthropogenic emissions which was probably
348 responsible for large drop of GEM from 2017 to 2018. Overall, the relative contribution of natural
349 surface emissions to ambient GEM was on the rise, e.g., from 3641% in 2015 to 5357% in 2018 on
350 annual average (Figures 76e & 76f).

351

352 4. Conclusions and Implications

353 Through a four-year continuous measurement of GEM in the suburbs of Shanghai, a clear
354 decreasing trend was observed with the rate of $-0.32 \pm 0.07 \text{ ng m}^{-3} \text{ yr}^{-1}$, which was mainly due to the
355 reduction of anthropogenic mercury emissions. The lower decreasing rate in warm seasons than in
356 cold seasons and the high correlation between GEM concentrations and temperature suggested that
357 natural surface emissions significantly impacted the GEM concentrations. By demonstrating that
358 temperature, O₃, and NH₃ can well serve as tracers of natural surface mercury emissions,
359 distinguishing natural vs. anthropogenic contributions to GEM was doable by introducing these
360 tracers into the PMF model. The results indicated that the contribution from anthropogenic mercury
361 emissions was declining, especially from coal combustion. The annual absolute contributions of
362 natural surface emissions were in the range of $1.00\text{-}1.13\text{-}0.90\text{-}1.01 \text{ ng/m}^3$, and the relative
363 contribution of natural surface emissions to GEM increasing from 3641% in 2015 to 5357% in 2018.

364 Measurements of GEM and other pollutants in a regional background area in Eastern China
365 demonstrated the effectiveness of emission control policies in this and surrounding regions in China
366 in recent years. The decreasing contributions from anthropogenic sources and the relatively stable

367 contributions from natural surface emissions to the ambient GEM have resulted in the relative
368 contributions of natural surface emissions surpassing those of anthropogenic emissions in more
369 recent years. This trend will likely continue for some years considering the current pollution levels
370 in China which needs further pollution abatement. This implies that even though the anthropogenic
371 emissions of mercury would continue to decrease, the legacy mercury in the natural surfaces will
372 continue to emit steadily for a long period of time. In addition, the natural release of mercury could
373 be enhanced under climate warming scenario. Hence, the atmospheric mercury concentration in
374 YRD or other parts of China will remain at relatively high levels in the near future, which brings
375 big challenges to China's policies on mercury emissions reduction. The methodology developed in
376 the present study could also shed some light on source apportionment of atmospheric mercury in
377 the other regions of the world, and has potential for improving emission databases from natural
378 surfaces where ambient GEM and auxiliary data are available.

379

380 **Acknowledgments**

381 The authors acknowledge support of the National Key R&D Program of China (2018YFC0213105),
382 the National Natural Science Foundation of China (91644105, 21777029), and the Natural Science
383 Foundation of Shanghai (18230722600,19ZR1421100).

384

385 **Author contribution**

386 X.Q. and K. H. designed this study. X.Q. performed measurements and data analysis. X.W., Q.F.,
387 Q.Z., Y.L., and J.H. performed data collection. X.Q., L.Z., K.H., and C.D. wrote the paper. All have
388 commented and reviewed the paper.

389

390 **Competing interests**

391 The authors declare that they have no conflict of interest.

392

393 **Data availability**

394 All data used in this study can be requested from K.H. (huangkan@fudan.edu.cn).

395

396 **References:**

397 Carslaw, D., Beevers, S., Ropkins, K., and Bell, M.: Detecting and quantifying aircraft and other on-
398 airport contributions to ambient nitrogen oxides in the vicinity of a large international airport,
399 *Atmospheric Environment*, 40, 5424-5434, 10.1016/j.atmosenv.2006.04.062, 2006.

400 Carslaw, D. C., and Ropkins, K.: openair — An R package for air quality data analysis, *Environmental*
401 *Modelling & Software*, 27-28, 52-61, 10.1016/j.envsoft.2011.09.008, 2012.

402 Chang, Y., Zou, Z., Deng, C., Huang, K., Collett, J. L., Lin, J., and Zhuang, G.: The importance of vehicle
403 emissions as a source of atmospheric ammonia in the megacity of Shanghai, *Atmospheric Chemistry and*
404 *Physics*, 16, 3577-3594, 10.5194/acp-16-3577-2016, 2016.

405 Chang, Y., Deng, C., Cao, F., Cao, C., Zou, Z., Liu, S., Lee, X., Li, J., Zhang, G., and Zhang, Y.:
406 Assessment of carbonaceous aerosols in Shanghai, China - Part 1: long-term evolution, seasonal
407 variations, and meteorological effects, *Atmospheric Chemistry and Physics*, 17, 9945-9964, 10.5194/acp-
408 17-9945-2017, 2017.

409 Cheng, I., Xu, X., and Zhang, L.: Overview of receptor-based source apportionment studies for speciated
410 atmospheric mercury, *Atmos. Chem. Phys.*, 15, 7877-7895, 10.5194/acp-15-7877-2015, 2015.

411 Clarkson, T. W., and Magos, L.: The toxicology of mercury and its chemical compounds, *Crit. Rev.*
412 *Toxicol.*, 36, 609-662, 10.1080/10408440600845619, 2006.

413 Driscoll, C. T., Mason, R. P., Chan, H. M., Jacob, D. J., and Pirrone, N.: Mercury as a global pollutant:
414 sources, pathways, and effects, *Environmental science & technology*, 47, 4967-4983, 10.1021/es305071v,
415 2013a.

416 Driscoll, C. T., Mason, R. P., Chan, H. M., Jacob, D. J., and Pirrone, N.: Mercury as a Global Pollutant:
417 Sources, Pathways, and Effects, *Environmental science & technology*, 47, 4967-4983, 2013b.

418 Duan, L., Wang, X., Wang, D., Duan, Y., Cheng, N., and Xiu, G.: Atmospheric mercury speciation in
419 Shanghai, China, *Sci. Total Environ.*, 578, 460-468, <https://doi.org/10.1016/j.scitotenv.2016.10.209>,
420 2017.

421 Feng, X. B., Wang, S. F., Qiu, G. A., Hou, Y. M., and Tang, S. L.: Total gaseous mercury emissions from
422 soil in Guiyang, Guizhou, China, *J. Geophys. Res.-Atmos.*, 110, 2005.

423 Friedli, H. R., Arellano, A. F., Cinnirella, S., and Pirrone, N.: Initial Estimates of Mercury Emissions to
424 the Atmosphere from Global Biomass Burning, *Environmental science & technology*, 43, 3507-3513,
425 10.1021/es802703g, 2009.

426 Fu, X. W., Feng, X. B., Sommar, J., and Wang, S. F.: A review of studies on atmospheric mercury in
427 China, *Sci. Total Environ.*, 421, 73-81, 10.1016/j.scitotenv.2011.09.089, 2012.

428 Gibson, M. D., Haelssig, J., Pierce, J. R., Parrington, M., Franklin, J. E., Hopper, J. T., Li, Z., and Ward,
429 T. J.: A comparison of four receptor models used to quantify the boreal wildfire smoke contribution to
430 surface PM_{2.5} in Halifax, Nova Scotia during the BORTAS-B experiment, *Atmospheric Chemistry and*
431 *Physics*, 15, 815-827, 10.5194/acp-15-815-2015, 2015.

432 Gustin, M. S., Lindberg, S. E., and Weisberg, P. J.: An update on the natural sources and sinks of
433 atmospheric mercury, *Appl. Geochem.*, 23, 482-493, 10.1016/j.apgeochem.2007.12.010, 2008.

434 Horowitz, H. M., Jacob, D. J., Zhang, Y., Dibble, T. S., Slemr, F., Amos, H. M., Schmidt, J. A., Corbitt,
435 E. S., Marais, E. A., and Sunderland, E. M.: A new mechanism for atmospheric mercury redox chemistry:
436 implications for the global mercury budget, *Atmospheric Chemistry and Physics*, 17, 6353-6371,
437 10.5194/acp-17-6353-2017, 2017.

438 Howard, D., and Edwards, G. C.: Mercury fluxes over an Australian alpine grassland and observation of
439 nocturnal atmospheric mercury depletion events, *Atmospheric Chemistry and Physics*, 18, 129-142, 2018.

440 Kerr, G. H., and Waugh, D. W.: Connections between summer air pollution and stagnation,

441 Environmental Research Letters, 13, 10.1088/1748-9326/aad2e2, 2018.

442 Kerr, G. H., Waugh, D. W., Strode, S. A., Steenrod, S. D., Oman, L. D., and Strahan, S. E.: Disentangling
443 the Drivers of the Summertime Ozone-Temperature Relationship Over the United States, 124, 10503-
444 10524, 10.1029/2019jd030572, 2019.

445 Kocman, D., Horvat, M., Pirrone, N., and Cinnirella, S.: Contribution of contaminated sites to the global
446 mercury budget, Environmental Research, 125, 160-170, 10.1016/j.envres.2012.12.011, 2013.

447 Landis, M. S., and Keeler, G. J.: Atmospheric mercury deposition to Lake Michigan during the Lake
448 Michigan Mass Balance Study, Environmental science & technology, 36, 4518-4524, 10.1021/es011217b,
449 2002.

450 Lindberg, S. E., Zhang, H., Vette, A. F., Gustin, M. S., Barnett, M. O., and Kuiken, T.: Dynamic flux
451 chamber measurement of gaseous mercury emission fluxes over soils: Part 2 - effect of flushing flow rate
452 and verification of a two-resistance exchange interface simulation model, Atmospheric Environment, 36,
453 847-859, 10.1016/s1352-2310(01)00502-7, 2002.

454 Liu, K., Wu, Q., Wang, L., Wang, S., Liu, T., Ding, D., Tang, Y., Li, G., Tian, H., Duan, L., Wang, X., Fu,
455 X., Feng, X., and Hao, J.: Measure-Specific Effectiveness of Air Pollution Control on China's
456 Atmospheric Mercury Concentration and Deposition during 2013-2017, Environmental science &
457 technology, 10.1021/acs.est.9b02428, 2019a.

458 Liu, K., Wu, Q., Wang, L., Wang, S., Liu, T., Ding, D., Tang, Y., Li, G., Tian, H., Duan, L., Wang, X., Fu,
459 X., Feng, X., and Hao, J.: Measure-Specific Effectiveness of Air Pollution Control on China's
460 Atmospheric Mercury Concentration and Deposition during 2013-2017, Environmental science &
461 technology, 53, 8938-8946, 10.1021/acs.est.9b02428, 2019b.

462 Mao, H., Talbot, R. W., Sigler, J. M., Sive, B. C., and Hegarty, J. D.: Seasonal and diurnal variations of
463 Hg degrees over New England, Atmospheric Chemistry and Physics, 8, 1403-1421, 10.5194/acp-8-1403-
464 2008, 2008.

465 Mason, R. P., and Sheu, G. R.: Role of the ocean in the global mercury cycle, Global Biogeochemical
466 Cycles, 16, 40-41-40-14, 10.1029/2001gb001440, 2002.

467 Mason, R. P.: Mercury Emissions from Natural Processes and their Importance in the Global Mercury
468 Cycle, Mercury Fate and Transport in the Global Atmosphere: Emissions, Measurements and Models,
469 edited by: Pirrone, N., and Mason, R., 173-191 pp., 2009.

470 Moore, C., and Carpi, A.: Mechanisms of the emission of mercury from soil: Role of UV radiation, J.
471 Geophys. Res.-Atmos., 110, 10.1029/2004jd005567, 2005.

472 Pannu, R., Siciliano, S. D., and O'Driscoll, N. J.: Quantifying the effects of soil temperature, moisture
473 and sterilization on elemental mercury formation in boreal soils, Environmental Pollution, 193, 138-146,
474 10.1016/j.envpol.2014.06.023, 2014.

475 Pirrone, N., Cinnirella, S., Feng, X., Finkelman, R. B., Friedli, H. R., Leaner, J., Mason, R., Mukherjee,
476 A. B., Stracher, G. B., Streets, D. G., and Telmer, K.: Global mercury emissions to the atmosphere from
477 anthropogenic and natural sources, Atmos. Chem. Phys., 10, 5951-5964, 10.5194/acp-10-5951-2010,
478 2010.

479 Poissant, L., and Casimir, A.: Water-air and soil-air exchange rate of total gaseous mercury measured at
480 background sites, Atmospheric Environment, 32, 883-893, 10.1016/s1352-2310(97)00132-5, 1998.

481 Polissar, A. V., Hopke, P. K., and Paatero, P.: Atmospheric aerosol over Alaska - 2. Elemental composition
482 and sources, J. Geophys. Res.-Atmos., 103, 19045-19057, 10.1029/98jd01212, 1998.

483 Qin, X., Wang, X., Shi, Y., Yu, G., Zhao, N., Lin, Y., Fu, Q., Wang, D., Xie, Z., Deng, C., and Huang, K.:
484 Characteristics of atmospheric mercury in a suburban area of east China: sources, formation mechanisms,

485 and regional transport, *Atmos. Chem. Phys.*, 19, 5923-5940, 10.5194/acp-19-5923-2019, 2019.

486 Quinones, J. L., and Anthony, C. J. J. o. E. Q.: An Investigation of the Kinetic Processes Influencing

487 Mercury Emissions from Sand and Soil Samples of Varying Thickness, 40, 647-, 2011.

488 Schnell, J. L., and Prather, M. J.: Co-occurrence of extremes in surface ozone, particulate matter, and

489 temperature over eastern North America, 114, 2854-2859, 10.1073/pnas.1614453114 %J Proceedings of

490 the National Academy of Sciences, 2017.

491 Schroeder, W. H., and Munthe, J.: Atmospheric mercury - An overview, *Atmospheric Environment*, 32,

492 809-822, 10.1016/s1352-2310(97)00293-8, 1998.

493 Sommar, J., Zhu, W., Shang, L., Lin, C.-J., and Feng, X.: Seasonal variations in metallic mercury (Hg-0)

494 vapor exchange over biannual wheat-corn rotation cropland in the North China Plain, *Biogeosciences*,

495 13, 2029-2049, 10.5194/bg-13-2029-2016, 2016.

496 Song, S., Selin, N. E., Soerensen, A. L., Angot, H., Artz, R., Brooks, S., Brunke, E. G., Conley, G.,

497 Dommergue, A., Ebinghaus, R., Holsen, T. M., Jaffe, D. A., Kang, S., Kelley, P., Luke, W. T., Magand,

498 O., Marumoto, K., Pfaffhuber, K. A., Ren, X., Sheu, G. R., Slemr, F., Warneke, T., Weigelt, A., Weiss-

499 Penzias, P., Wip, D. C., and Zhang, Q.: Top-down constraints on atmospheric mercury emissions and

500 implications for global biogeochemical cycling, *Atmospheric Chemistry and Physics*, 15, 7103-7125,

501 10.5194/acp-15-7103-2015, 2015.

502 Streets, D. G., Devane, M. K., Lu, Z. F., Bond, T. C., Sunderland, E. M., and Jacob, D. J.: All-Time

503 Releases of Mercury to the Atmosphere from Human Activities, *Environmental science & technology*,

504 45, 10485-10491, 10.1021/es202765m, 2011.

505 Tang, Y., Wang, S. X., Wu, Q. R., Liu, K. Y., Wang, L., Li, S., Gao, W., Zhang, L., Zheng, H. T., Li, Z.

506 J., and Hao, J. M.: Recent decrease trend of atmospheric mercury concentrations in East China: the

507 influence of anthropogenic emissions, *Atmospheric Chemistry and Physics*, 18, 8279-8291, 10.5194/acp-

508 18-8279-2018, 2018.

509 Wang, D. Y., He, L., Shi, X. J., Wei, S. Q., and Feng, X. B.: Release flux of mercury from different

510 environmental surfaces in Chongqing, China, *Chemosphere*, 64, 1845-1854,

511 10.1016/j.chemosphere.2006.01.054, 2006.

512 Wang, L., Wang, S. X., Zhang, L., Wang, Y. X., Zhang, Y. X., Nielsen, C., McElroy, M. B., and Hao, J.

513 M.: Source apportionment of atmospheric mercury pollution in China using the GEOS-Chem model,

514 *Environmental Pollution*, 190, 166-175, 10.1016/j.envpol.2014.03.011, 2014a.

515 Wang, X., Lin, C. J., and Feng, X.: Sensitivity analysis of an updated bidirectional air-surface exchange

516 model for elemental mercury vapor, *Atmospheric Chemistry and Physics*, 14, 6273-6287, 10.5194/acp-

517 14-6273-2014, 2014b.

518 Wang, X., Lin, C.-J., Yuan, W., Sommar, J., Zhu, W., and Feng, X.: Emission-dominated gas exchange

519 of elemental mercury vapor over natural

520 surfaces in China, *Atmospheric Chemistry and Physics*, 16, 11125-11143, 10.5194/acp-16-11125-2016,

521 2016.

522 Wright, L. P., and Zhang, L. M.: An approach estimating bidirectional air-surface exchange for gaseous

523 elemental mercury at AMNet sites, *Journal of Advances in Modeling Earth Systems*, 7, 35-49,

524 10.1002/2014ms000367, 2015.

525 Wright, L. P., Zhang, L., Cheng, I., Aherne, J., and Wentworth, G. R.: Impacts and Effects Indicators of

526 Atmospheric Deposition of Major Pollutants to Various Ecosystems - A Review, *Aerosol Air Qual. Res.*,

527 18, 1953-1992, 10.4209/aaqr.2018.03.0107, 2018.

528 Wu, Q. R., Wang, S. X., Li, G. L., Liang, S., Lin, C. J., Wang, Y. F., Cai, S. Y., Liu, K. Y., and Hao, J. M.:

529 Temporal Trend and Spatial Distribution of Speciated Atmospheric Mercury Emissions in China During
530 1978-2014, *Environmental science & technology*, 50, 13428-13435, 10.1021/acs.est.6b04308, 2016.

531 Wu, Y., Wang, S. X., Streets, D. G., Hao, J. M., Chan, M., and Jiang, J. K.: Trends in anthropogenic
532 mercury emissions in China from 1995 to 2003, *Environmental science & technology*, 40, 5312-5318,
533 10.1021/es060406x, 2006.

534 Xu, X., Liao, Y., Cheng, I., and Zhang, L.: Potential sources and processes affecting speciated
535 atmospheric mercury at Kejimikujik National Park, Canada: comparison of receptor models and data
536 treatment methods, *Atmospheric Chemistry and Physics*, 17, 1381-1400, 10.5194/acp-17-1381-2017,
537 2017.

538 Xu, X. H., Yang, X. S., Miller, D. R., Helble, J. J., and Carley, R. J.: Formulation of bi-directional
539 atmosphere-surface exchanges of elemental mercury, *Atmospheric Environment*, 33, 4345-4355,
540 10.1016/s1352-2310(99)00245-9, 1999.

541 Yu, Y., He, S., Wu, X., Zhang, C., Yao, Y., Liao, H., Wang, Q., and Xie, M.: PM2.5 elements at an urban
542 site in Yangtze River Delta, China: High time-resolved measurement and the application in source
543 apportionment, *Environ Pollut*, 253, 1089-1099, 10.1016/j.envpol.2019.07.096, 2019.

544 Zhang, L., Wright, L. P., and Asman, W. A. H.: Bi-directional air-surface exchange of atmospheric
545 ammonia: A review of measurements and a development of a big-leaf model for applications in regional-
546 scale air-quality models, *J. Geophys. Res.-Atmos.*, 115, 10.1029/2009jd013589, 2010.

547 Zhang, L., Wang, S. X., Meng, Y., and Hao, J. M.: Influence of Mercury and Chlorine Content of Coal
548 on Mercury Emissions from Coal-Fired Power Plants in China, *Environmental science & technology*, 46,
549 6385-6392, 10.1021/es300286n, 2012.

550 Zhang, L., Wang, S., Wang, L., Wu, Y., Duan, L., Wu, Q., Wang, F., Yang, M., Yang, H., Hao, J., and Liu,
551 X.: Updated emission inventories for speciated atmospheric mercury from anthropogenic sources in
552 China, *Environmental science & technology*, 49, 3185-3194, 10.1021/es504840m, 2015.

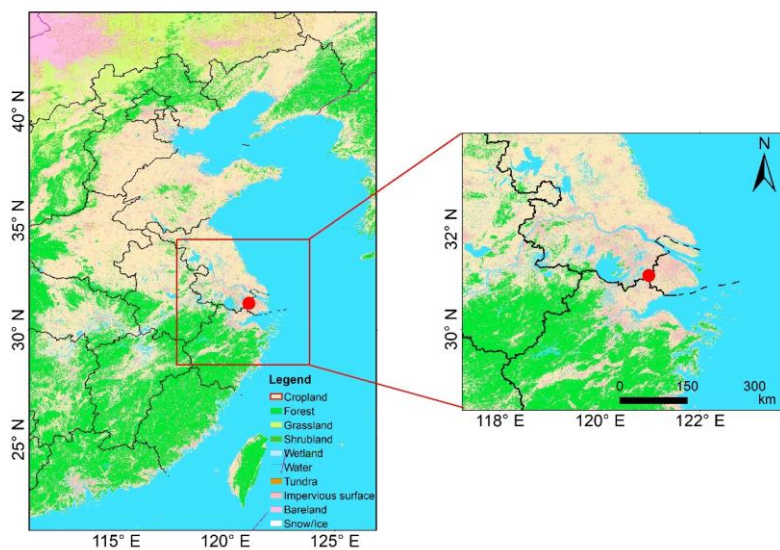
553 Zhang, Y., Jacob, D. J., Horowitz, H. M., Chen, L., Amos, H. M., Krabbenhoft, D. P., Slemr, F., St Louis,
554 V. L., and Sunderland, E. M.: Observed decrease in atmospheric mercury explained by global decline in
555 anthropogenic emissions, *Proc Natl Acad Sci U S A*, 113, 526-531, 10.1073/pnas.1516312113, 2016.

556 Zheng, B., Tong, D., Li, M., Liu, F., Hong, C., Geng, G., Li, H., Li, X., Peng, L., Qi, J., Yan, L., Zhang,
557 Y., Zhao, H., Zheng, Y., He, K., and Zhang, Q.: Trends in China's anthropogenic emissions since 2010 as
558 the consequence of clean air actions, *Atmospheric Chemistry and Physics*, 18, 14095-14111,
559 10.5194/acp-18-14095-2018, 2018.

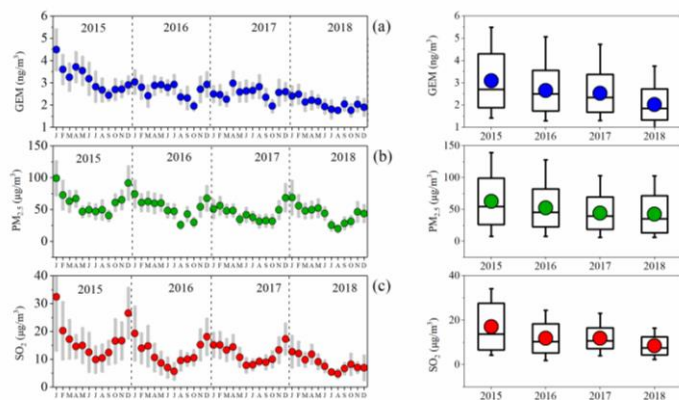
560 Zheng, J., Jiang, P., Qiao, W., Zhu, Y., and Kennedy, E.: Analysis of air pollution reduction and climate
561 change mitigation in the industry sector of Yangtze River Delta in China, *Journal of Cleaner Production*,
562 114, 314-322, 10.1016/j.jclepro.2015.07.011, 2016.

563 Zhu, W., Sommar, J., Lin, C. J., and Feng, X.: Mercury vapor air-surface exchange measured by
564 collocated micrometeorological and enclosure methods - Part II: Bias and uncertainty analysis,
565 *Atmospheric Chemistry and Physics*, 15, 5359-5376, 10.5194/acp-15-5359-2015, 2015.

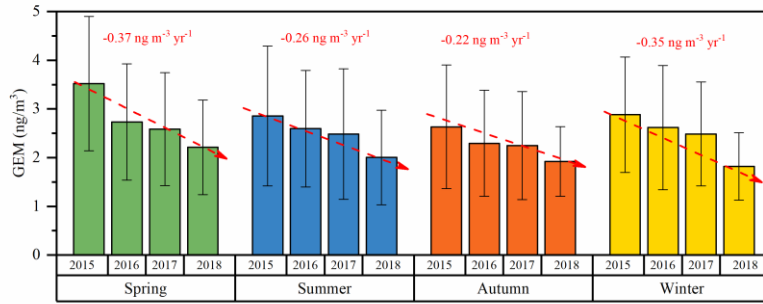
566 Zhu, W., Lin, C.-J., Wang, X., Sommar, J., Fu, X., and Feng, X.: Global observations and modeling of
567 atmosphere-surface exchange of elemental mercury: a critical review, *Atmospheric Chemistry and
568 Physics*, 16, 4451-4480, 10.5194/acp-16-4451-2016, 2016.



570 Figure 1. The location of the Dianshan Lake (DSL) site in Shanghai, China. Different colors in the
 571 map represent different land cover types.
 572



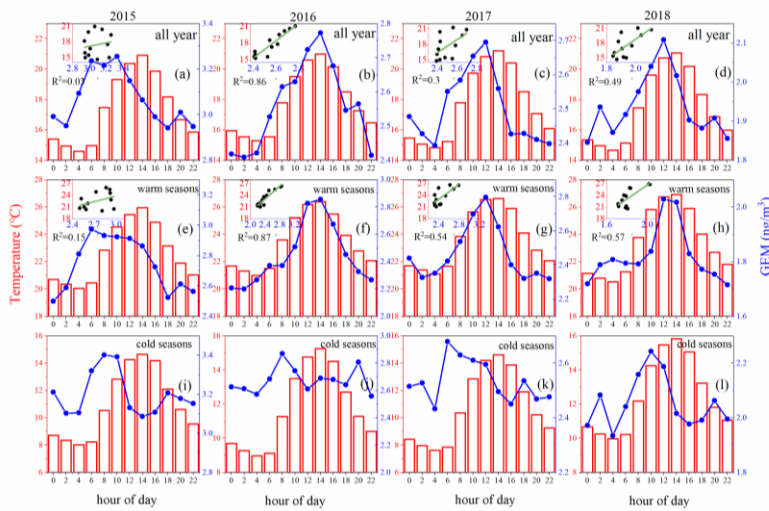
573
 574 Figure 2. Monthly and annual variations of (a) GEM, (b) $PM_{2.5}$, and (c) SO_2 concentrations from
 575 2015 to 2018.
 576



578 Figure 3. Seasonal variations of GEM concentrations from 2015 to 2018. The variation rates of
 579 GEM for each season are also shown in the figure.

580

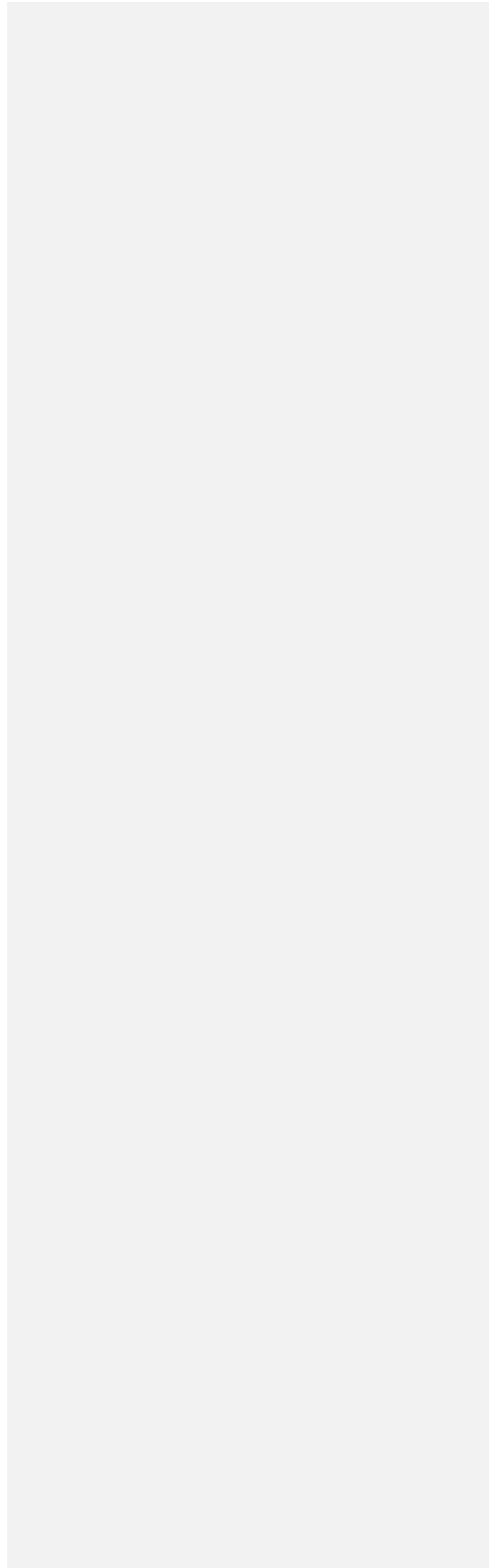
581

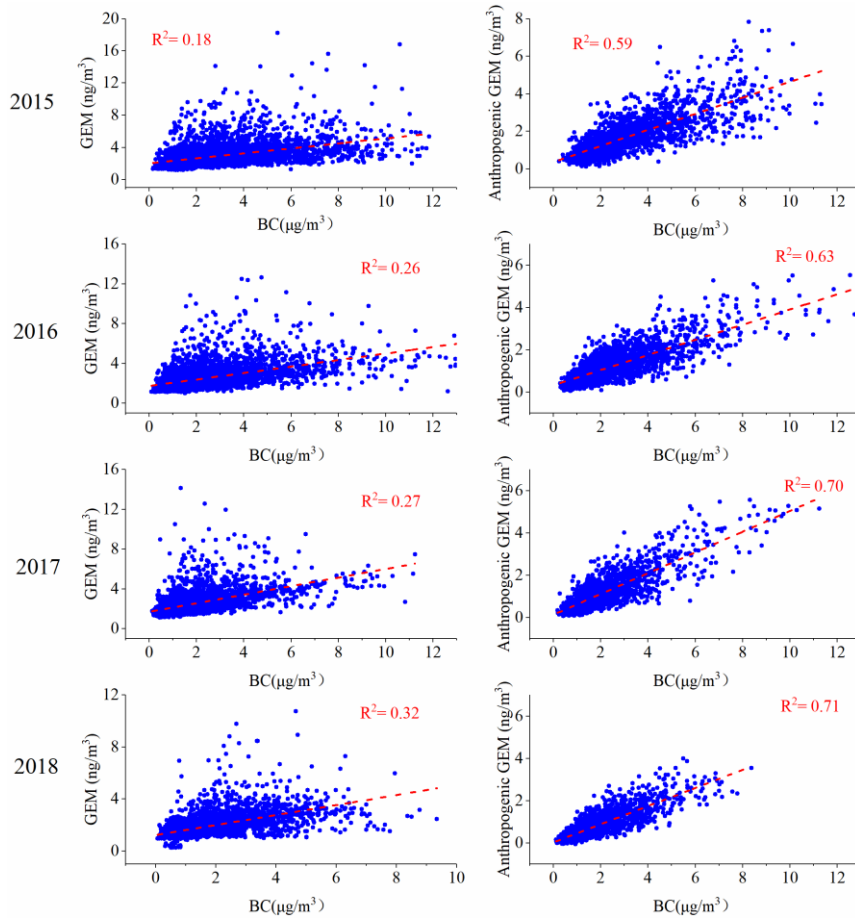


582 Figure 4. Diurnal patterns of bi-hourly GEM concentrations and temperature for the whole year (a-
 583 d), warm seasons (e-h), and cold seasons (i-l) during 2015 – 2018, respectively. The linear
 584 correlations between GEM and temperature are inserted as inner figures.

585

586





589

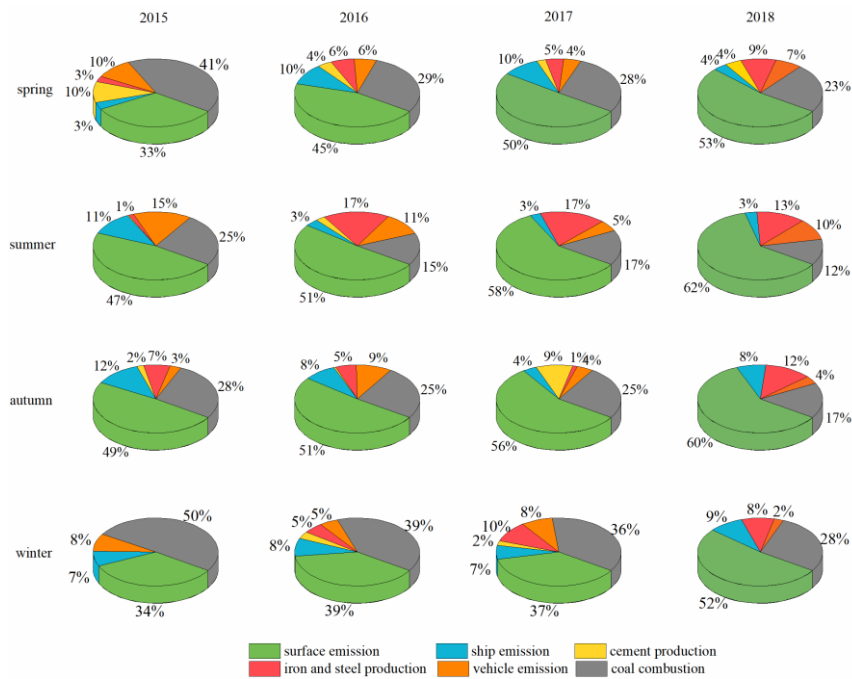
590 Figure 5. The relationship between observed GEM and BC, anthropogenic GEM (extracted from591 PMF results) and BC during 2015 – 2018

592

593

594

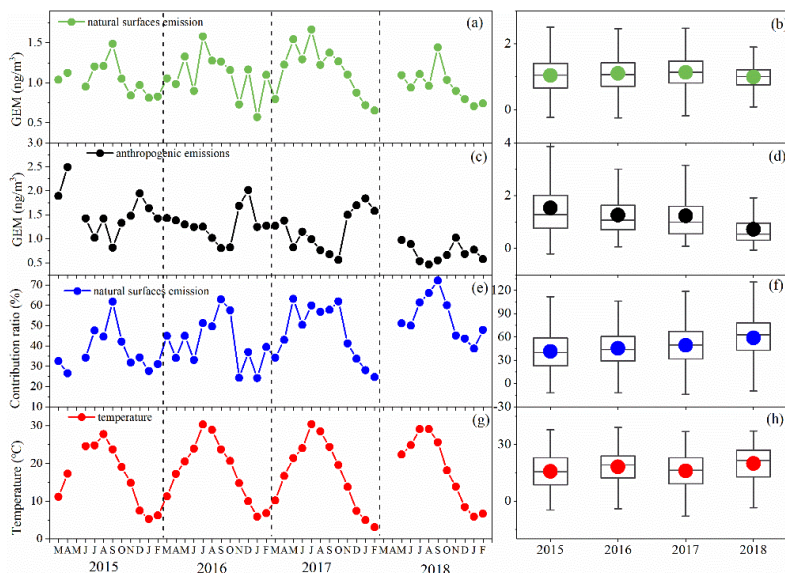
595



596
597
598
599
600
601
602
603
604

Formatted: English (Canada)

Figure 65. Contributions of natural surface emissions and anthropogenic sources to atmospheric GEM in the four seasons during 2015 – 2018.



605
606

607 Figure 76. The monthly and annual GEM concentrations contributed by natural surface emissions
608 (a-b) and anthropogenic emissions (c-d) from 2015 to 2018. (e-f) The monthly and annual
609 contribution of natural surface emissions to GEM concentrations from 2015 to 2018. (g-h) The
610 corresponding ambient temperature from 2015 to 2018.